Advanced Materials

ADVANCED MATERIALS
www.advmat.de

RESEARCH ARTICLE OPEN ACCESS

Bubble Formation Control: Fabrication of Centimeter-Sized Tissue-Like Constructs by Catalase-Coated Oxygen-Releasing Hydrogel

Sukulya Bunuasunthon[1] | Isabel F. Amaral[2,3] | Ana P. Pêgo[2,3,4] | Michiya Matsusaki[1]

[1]Department of Applied Chemistry, Graduate School of Engineering, The University of Osaka, Suita, Osaka, Japan | [2]i3S – Instituto de Investigação e Inovação em Saúde, Universidade do Porto, Porto, Portugal | [3]INEB – Instituto de Engenharia Biomédica, Universidade do Porto, Porto, Portugal | [4]ICBAS – Instituto de Ciências Biomédicas Abel Salazar, Universidade do Porto, Portugal

Correspondence: Ana P. Pêgo (apego@i3s.up.pt) | Michiya Matsusaki (m-matsus@chem.eng.osaka-u.ac.jp)

Received: 26 November 2025 | **Revised:** 28 May 2026 | **Accepted:** 2 June 2026

Keywords: calcium peroxide | catalase enzyme | centimeter-size scaffold | human neural stem cells | oxygen-releasing material

ABSTRACT

Developing thick three-dimensional (3D) scaffolds remains challenging due to oxygen depletion and limited cell viability. Calcium peroxide (CaO_2)-catalase-based oxygen-releasing biomaterials are a common solution, but the uncontrolled release of oxygen bubbles often leading to structural damages is rarely discussed. Herein, we present a strategy to control the site of bubble formation in an oxygen-releasing hydrogel, by applying a catalase nanocoating to its surface. CaO_2 undergoes hydrolytic decomposition with water, generating hydrogen peroxide (H_2O_2), subsequently converts into O_2 and H_2O. Because H_2O_2 can induce cytotoxicity, direct catalase incorporation into hydrogel systems may accelerate O_2 bubble formation, leading in hydrogel collapse within 1 h of aqueous immersion. In comparison, catalase-coated hydrogels exhibited improved structural stability, showing a 5.9-fold smaller bubble size than hydrogels with mixed catalase after 24 h in ambient air. Under hypoxic conditions ($O_2 < 0.1\%$), centimeter-scale constructs containing catalase-coated hydrogels preserved up to 86% viable human fibroblast cells after 5 days of culture, compared with only 47% in non-catalase coated hydrogels. Furthermore, the incorporation of catalase-coated hydrogels promoted cell survival and neurite outgrowth of human neural stem cells cultured in neuronal differentiation conditions under severe hypoxia. These findings suggest the potential of the proposed strategy for oxygen-supportive tissue engineering applications.

1 | Introduction

Organ damage and failure are among the leading causes of death worldwide [1]. Organ transplantation remains one of the most effective treatment options but the availability of compatible donors often fails to meet the demand. Therefore, tissue engineering, particularly the fabrication of three-dimensional (3D) tissues or organs has emerged as a promising alternative for organ and tissue regeneration [2–4]. Cell survival inside these 3D tissue-engineered constructs is essential for proliferation, functional maintenance, and metabolic processes. Nevertheless, several challenges remain in both the pre- and post-fabrication stages of engineered tissues, including maintaining high cell viability in thick constructs [5, 6], achieving sufficient cell proliferation [7], and sustaining adequate metabolic activity within the scaffold [8]. Numerous studies have demonstrated that constructs thicker than 100 μm often suffer from limited oxygen and nutrient diffusion, compromising cellular function [9]. While mild oxygen deprivation can alter cell behavior, extreme hypoxia can lead to irreversible damage and cell death. Therefore, supplying oxygen in a thick tissue constructs, for example through introduction of vascular network, is essential for maintaining cell viability and

tissue function [10]. The initial research in this area relied on angiogenesis from the host side to generate a vascular network in the grafted tissue after transplantation [11]. Although this approach can promote vascularization during the initial phase, complete formation of a functional network within a 3-mm tissue construction typically requires 1–2 weeks post-implantation. During this period, the inner regions of the scaffold remain oxygen-deprived, often leading to extensive cell apoptosis and loss of viability [12].

Peroxide-based compounds are promising agents for localized oxygen generation within tissue-engineered constructs, helping to meet the oxygen demands of encapsulated cells [13–15]. Among these, calcium peroxide (CaO_2) is one of the most widely used materials [16, 17]. When CaO_2 reacts with water, it undergoes hydrolytic decomposition to produce hydrogen peroxide (H_2O_2) which subsequently breaks down into oxygen and water [18]. The interaction between a solid peroxide and an aqueous solution can occur rapidly, generating an initial burst release of oxygen and reactive oxygen species (ROS) which could be deleterious to cells [19]. To prevent this direct interaction, most studies have reported the encapsulation of the solid peroxide within a hydrophobic polymer matrix such as polycaprolactone (PCL), polylactic co-glycolic acid (PLGA), or poly(vinyl pyrrolidone) (PVP) [20]. However, these matrices are still limited by poor cell attachment [21] or risk of cell toxicity [22], restricting their use in tissue engineering to some extent. Beyond hydrophobic encapsulation, the use of Ca^{2+} ions derived from CaO_2 dissociation as ionic crosslinkers for hydrogel formation has also been reported [23]. Although this strategy minimizes direct contact between CaO_2 and its aqueous surroundings, it remains crucial to enhance the conversion of H_2O_2 into oxygen. Because H_2O_2 is cytotoxic, its excessive accumulation can induce oxidative stress and lead to cell apoptosis [24]. To prevent this, catalase has been widely applied to catalyzed H_2O_2 decomposition into water and oxygen, thereby promoting sustained oxygen release while preserving cell viability [25, 26]. To address this, most studies incorporate catalase enzyme using various approaches including covalent modification of the alginate backbone [27], addition in culture medium [28], or direct mixing during hydrogel formation [23, 29, 30]. This catalase-mediated oxygen generation often induces a rapid burst release, resulting in bubble formation that is indicative of H_2O_2 decomposition. However, this additional bubble formation may compromise hydrogel integrity, a drawback that remains largely overlooked in the literature. Although we previously demonstrated sustained oxygen release through hydroxyapatite (HAp) surface modification of CaO_2 particles [31], embedded HAp-CaO_2 microparticles in gelatin hydrogel together with catalase still led to noticeable bubble formation, which may limit their applicability in fabricating thick tissue scaffolds. Considering these challenges, we emphasize the importance of minimizing direct contact between CaO_2 and water and mitigating bubble formation during catalase mediated H_2O_2 decomposition.

Herein, we report the fabrication of an oxygen-releasing hydrogel through the selective interaction between CaO_2 and a functionalized biodegradable polymer, further incorporating catalase via a nanocoating strategy on the hydrogel surface. Inspired by previous CaO_2-mediated oxygen-releasing hydrogel [23], along with earlier work on HAp-CaO_2 microparticle [31] and on the development of a stabilized ionic-crosslinked hydrogel based on biodegradable poly(γ-glutamic acid) (γ-PGA) conjugated with alendronic acid (Aln) and L-phenylalanine (Phe) resulting in γ-PGA-Aln-Phe [32], we sought to integrate these concepts into a single system. By exploiting the bisphosphonate (BP) groups on Aln, known for their strong affinity to HAp [33], we then designed an oxygen-releasing hydrogel formed through specific interactions between HAp-coated CaO_2 and Aln moieties, which enabled sustained oxygen generation from CaO_2 decomposition. To enhance binding efficiency and gelation kinetics, nanoscale CaO_2 particles were used (Figure 1a). In parallel, recognizing that catalase plays a critical role in decomposing ROS [34] yet can induce structural instability when directly mixed into a hydrogel matrix [35], we developed a surface nanocoating strategy for catalase immobilization. Unlike conventional mixing, this localized approach allows controlled H_2O_2 decomposition, minimizes bubble formation, and preserves hydrogel integrity (Figure 1b). The material was initially assessed for its ability to support cell viability of normal human dermal fibroblasts (NHDFs) cultured within millimeter- and centimeter-scale fibrin scaffolds under hypoxic conditions. Having demonstrated its feasibility as an oxygen-supportive platform for thick tissue constructs, the system was further evaluated using human neural stem cells (hNSCs) cultured under neuronal differentiation conditions, where differentiating cells become increasingly dependent on oxidative phosphorylation for maturation [36–38]. The enhanced cell survival and increased neurite complexity observed under severe hypoxia condition in the presence of the catalase-coated hydrogel further support the potential of the materials as an oxygen-supportive platform for hNSC neuronal differentiation under deficient conditions.

This work describes a dual strategy combining selective polymer-particle interactions and catalase nanocoating to develop a structurally stable oxygen-releasing hydrogel platform capable of supporting cell survival under hypoxic conditions. In addition to its potential application for thick tissue engineering, the findings from this study may also advance the development of oxygen-supportive biomaterials capable of sustaining neural stem cell survival and neuronal differentiation under oxygen-deficient environments relevant to stroke and ischemic conditions [39].

2 | Results and Discussion

2.1 | Fabrication and Selective Interaction of Oxygen-Releasing Hydrogel

CaO_2 NPs were successfully prepared via hydrolysis precipitation method, yielding particle size of 150 ± 30 nm confirmed by scanning electron microscopy (SEM) and X-ray diffraction (XRD) presenting the characteristic CaO_2 reflections (Figure S1a,b). Bisphosphonate-functionalized γ-PGA polymers (γ-PGA-Aln) polymers with 10% to 40% [32] (Table S1) and examined for gelation with CaO_2 NPs. Upon mixing a CaO_2 dispersion with polymer solution, gelation occurred within 10 s (Supplementary Video S1), suggesting strong interactions between CaO_2 NPs and the γ-PGA-Aln polymer. This behavior is likely driven by Aln's high affinity for calcium ions and hydroxyapatite [40], which facilitated gel formation by promoting interactions on

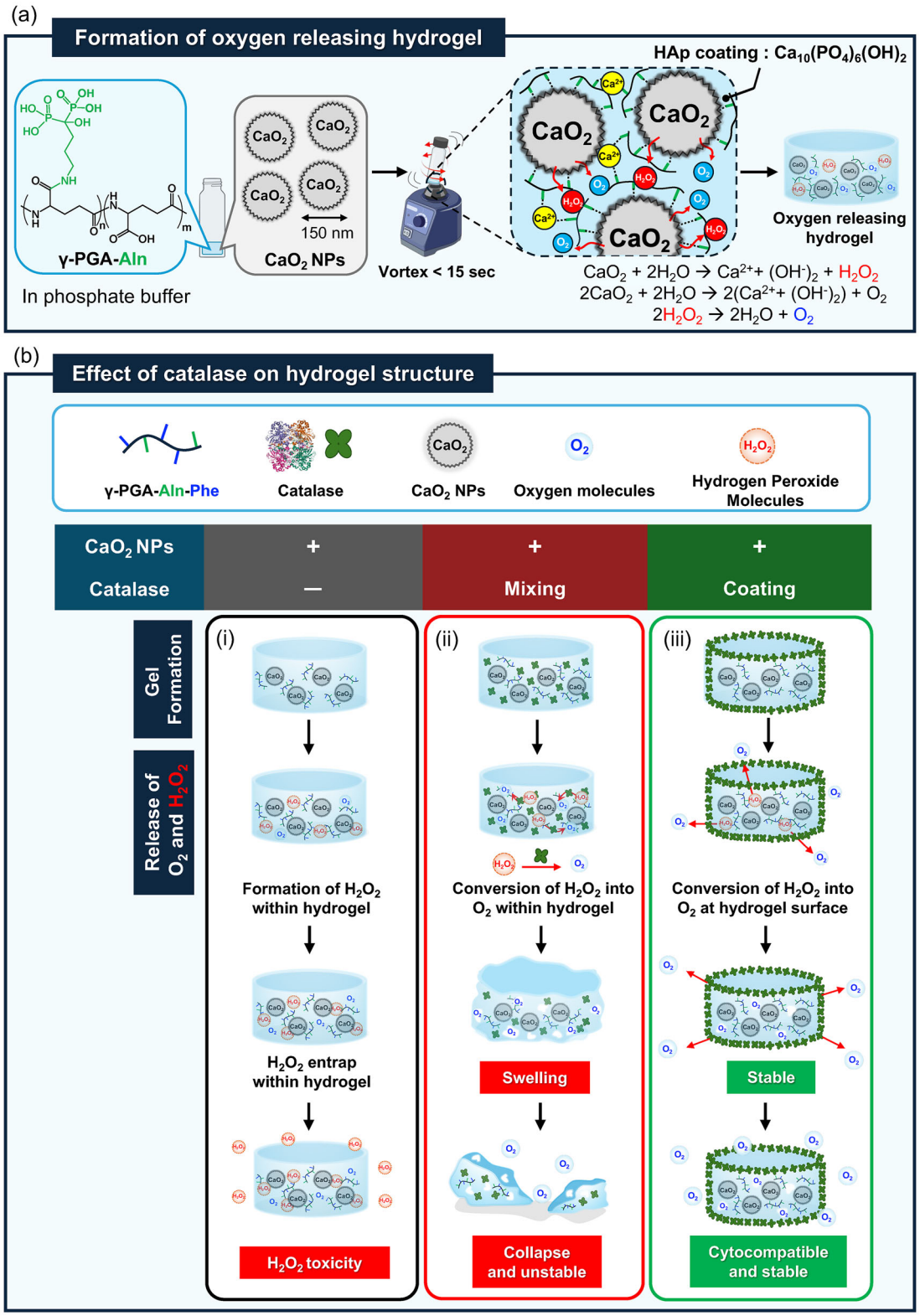

FIGURE 1 | Overview of work. (a) Schematic illustration of the preparation of oxygen-releasing hydrogels composed of γ-PGA-Aln polymer in phosphate buffer (PB) and dispersed of CaO_2 nanoparticles (NPs) in absolute ethanol. Gelation is initiated by vortexing, which promote CaO_2 NPs reaction with PB. This reaction forms a hydroxyapatite (HAp) surface that facilitates the interaction with γ-PGA-Aln, resulting in rapid gel formation. (b) Schematic representing different catalase incorporation techniques and their effect on the hydrogel structure. (i) A control oxygen-releasing hydrogel without catalase content. The decomposition of CaO_2 NPs generates hydrogen peroxide (H_2O_2) and O_2 within the hydrogel, which can induce toxicity. (ii) General mixing approach of catalase within the hydrogel. This approach can disrupt the material's stability and affect its swelling, due to the formation of additional O_2 within the hydrogel. (iii) Catalase coating strategy used in this study. This method allows catalase to localize at the hydrogel's surface, which effectively suppresses H_2O_2 accumulation within the hydrogel and assures the retention of the hydrogel stability over time.

the NP surface. Additionally, the partial dissociation of CaO_2 NPs during mixing may release Ca^{2+} ions, further reinforcing hydrogel network formation through ionic crosslinking [23, 41]. Systematic variation of grafting degree and CaO_2 NP content from 0.5 to 4 wt% revealed that hydrogel formation highly sensitive to the stoichiometry between the crosslinking sites (Aln) and the crosslinker (CaO_2 NPs) (Figure 2a,b). Excessive crosslinker concentration led to overly rapid aggregation, non-uniform network formation, and resulted in a decrease in the Young's modulus (Figure 2c). Therefore, the formulation of 10% w/w γ-PGA-Aln10 with a suspension of 1 wt% CaO_2 NPs was identified as optimal and used for further studies.

To assess selectivity, γ-PGA-Aln10 was compared with other polysaccharides, divalent cations, and peroxide compounds. As shown in Table S2, neither polysaccharide formed a uniform gel upon mixing with 1 wt% CaO_2 NPs, demonstrating the bisphosphonate groups from Aln are essential for initiating crosslinking. Unlike previous reports in which CaO_2 NPs were used as a secondary crosslinker in alginate-based systems [42], our strategy involves dissolving the polymer in phosphate buffer, which facilitates the formation of HAp on the surface of CaO_2 NPs [31]. This in situ HAp formation was hypothesized to be a major interaction for gelation followed by ionic crosslinking from released Ca^{2+}. The presence of HAp by XRD analysis of the dried hydrogel (Figure S2), supporting the HAp-bisphosphonate binding hypothesis (Figure 1a). The resulting CaO_2 NPs-based hydrogel exhibited superior properties compared to systems crosslinked with different divalent cations. Comparing between common divalent cations, only the mixture of γ-PGA-Aln10 with $MgCl_2$ resulted in a uniform, transparent hydrogel without residual unreacted polymer (Table S3). This observation aligns with findings from Topuz et al. [43]. suggesting that the slower interaction kinetics between Mg^{2+} and polysaccharides allow for the formation of more homogeneous hydrogel networks. Critically, at 1 min post-gelation, the CaO_2 NPs hydrogel displayed 10 times higher in Young's modulus than the $CaCl_2$-based system (Figure 2d), suggesting that the gelation base on CaO_2 NPs interaction could reinforce stronger binding within the hydrogel structure. While a reduction in Young's modulus of the oxygen-releasing hydrogel over time, likely due to internal oxygen bubble formation disrupting the gel structure and compromising mechanical integrity. Furthermore, we found that gelation was highly dependent on the peroxide type and particle size. As shown in Figure 2e, the use of micron-sized CaO_2 particles resulted in a markedly longer gelation time and 10-fold lower mechanical strength than the nanoscale particles. These findings emphasized that the nanoscale of CaO_2 and specific bisphosphonate-HAp interaction are key to achieving rapid and mechanically robust for fabrication of an oxygen-releasing hydrogel.

2.2 | Mechanical Optimization and Time-Dependent Bubble Formation in Oxygen-Releasing Hydrogel

The long-term functional stability of oxygen-releasing scaffolds is challenged by excessive bubble formation, which several studies used as an indicator of oxygen generation [35]. We first optimized the mechanical properties by comparing hydrogels formed from 10% w/w γ-PGA-Aln10 with varying concentrations of CaO_2 NPs (0.5, 1, and 2 wt%). Initial compression testing, after 1 min of fabrication, hydrogel containing 1 wt% CaO_2 NPs exhibited the highest strength of 33 kPa, followed by 30 and 14 kPa of 2 and 0.5 wt% CaO_2 NPs (Figure 2f). At longer incubation times, the Young's modulus of the oxygen-releasing hydrogel containing 1 wt% and 2 wt% gradually decreased over time, with values of 11 and 3 kPa after 24 h incubation. Interestingly, the hydrogel containing 0.5 wt% CaO_2 NPs showed a slight increase in Young's modulus after 1 h at room temperature, followed by a reduction after 24 h of incubation. These results support the hypothesis that a uniform oxygen-releasing hydrogel depends on carefully optimized conditions. A low concentration of CaO_2 NPs may be insufficient for complete gelation, while a high concentration may lead to excessive oxygen release. This can disrupt the hydrogel network and reduce its compressive strength over time. Since the hydrogel with 1 wt% CaO_2 NPs demonstrated a greater Young's modulus both initially and after 24 h than the other conditions, it was selected as the optimal concentration for the fabrication of oxygen-releasing hydrogels throughout the remainder of the study.

Accordingly, the effect of oxygen release on the polymer network over time was further evaluated through observations of the gel's macroscopic appearance using phase-contrast images, and SEM imaging, as shown in Figure 2g. After 24 h, the material showed visible swelling and surface bubbling, indicating ongoing oxygen release. Phase-contrast imaging of cross-sections further revealed the development of larger internal bubbles over time, suggesting increased oxygen accumulation within the hydrogel. Similarly, SEM imaging supported these findings. The presence of CaO_2 NPs within the material (indicated by yellow arrows) was clearly observed immediately after gelation but was no longer visible after 24 h, suggesting conversion of the particles. These observations were confirmed by SEM-EDS analysis (Figure 2h) where calcium signals were distinctly detected at 1 min post-gelation but only faintly present after 24 h. The bubbling size and the pore size within the matrix was then evaluated and calculated using ImageJ software (Figure 2i). Bubble size obtained from phase contrast imaging resulted in an average size of 132 μm initially and 177 μm after 24 h of incubation, representing a 1.3-fold increase in bubble size. Similarly, porosity measured from SEM images also reporteda corresponding increase of 1.4-fold after 24 h, from 0.71 μm to 0.99 μm. The increase in bubble diameter and pore size within the matrix indicates the success of oxygen conversion. However, this internal gas formation may disrupt and affect the compactness of the materials, leading to reduced material's stability.

2.3 | Influence of Phosphate Buffer and Conjugation of Hydrophobic Moieties for Long-Term Structural Stability

Considering the critical role of HAp layer in promoting bisphosphonate-mediated binding, we further evaluated the gelation ability of the system under different phosphate buffer (PB) concentrations, specifically comparing 500 mM and 1 M. XRD and SEM-EDS elemental mapping confirmed that preparation in 1 M PB enhanced HAp formation on the CaO_2 NP surface, evidenced by a more prominent phosphate peak and characteristic star-shaped crystalline structures (Figure S3a–d). These results

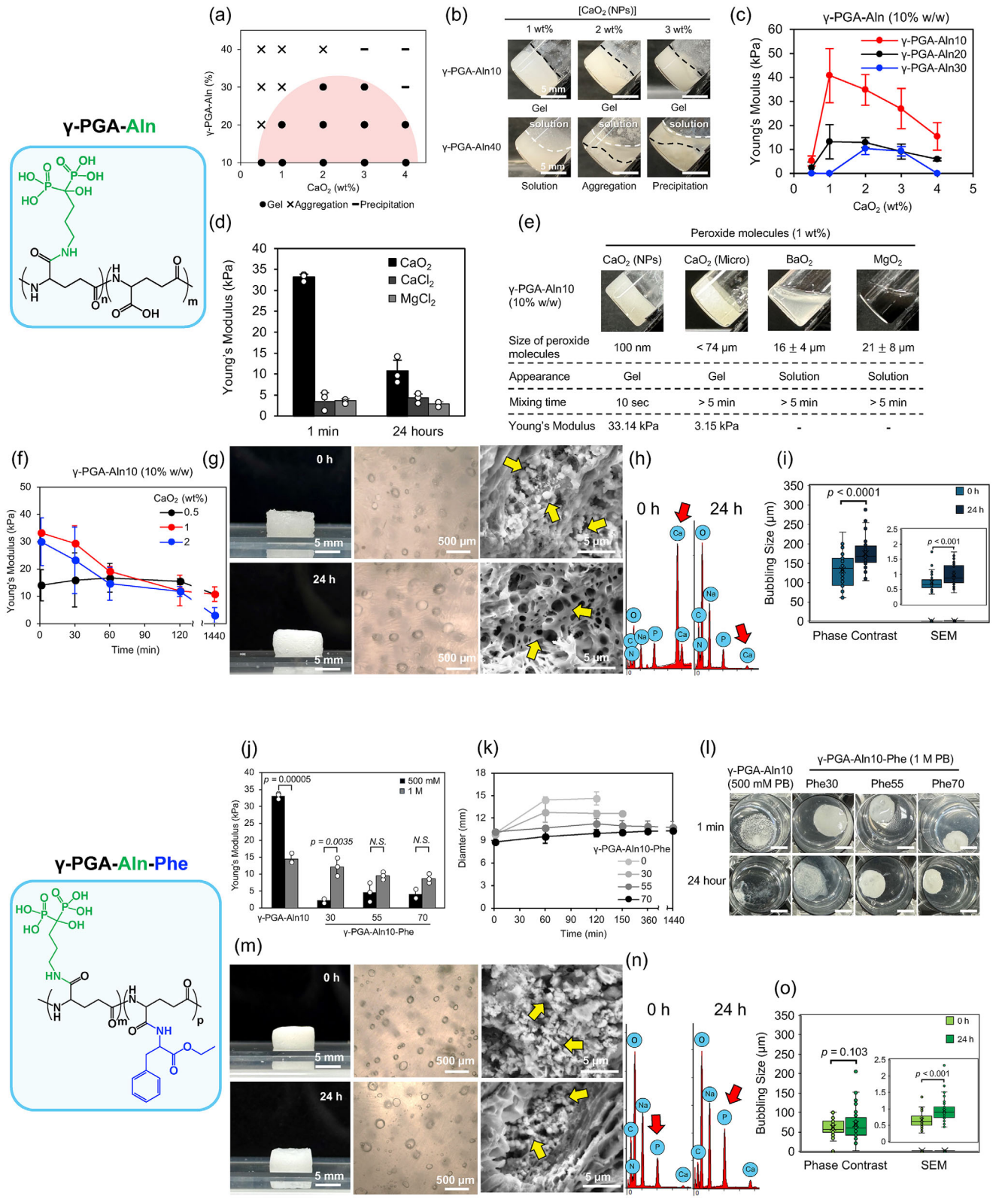

FIGURE 2 | Formation and characterization of oxygen-releasing hydrogels. Hydrogel construction using γ-PGA-Aln was evaluated under varying formulation conditions (a–i). (a) Gelation map of γ-PGA-Aln at different Aln grafting degrees and CaO_2 NPs concentrations, where red areas indicate successful gel formation. (b) Representative images of hydrogels under each condition (scale bar = 5 mm). (c) Compressive strength of hydrogels crosslinked with varying grafting degrees and CaO_2 NPs content. (d–e) Young's modulus of hydrogels crosslinked with different divalent ions and summary of peroxide-based gelation outcomes. (f) Time-dependent Young's modulus of 10% w/w γ-PGA-Aln10 hydrogels with 0.5–2 wt% CaO_2 NPs. (g) Representative macroscopic, phase contrast, and SEM images of cross-sectioned 10% w/w γ-PGA-Aln10 with 1 wt% CaO_2 NPs hydrogel at 0 h and 24 h. (h) Elemental composition from SEM-EDS analysis within the constructed hydrogels at the site of the SEM image (yellow arrow) at 0 h and 24 h. (i) Quantification of bubble sizes within hydrogels at 0 h and 24 h using phase contrast and SEM imaging. Data are summarized from three independent

support the hypothesis that the Aln group selectively interacts with HAp-coated CaO_2, promoting gelation via bisphosphonate-mediated binding.

Building on the need for stability in aqueous environment, we introduced phenylalanine grafts into the polymer backbone, yielding γ-PGA-Aln10-Phe polymers with varying degrees of substitution, ranging from Phe30 to Phe70 (Table S4). Interestingly, hydrogels formed from γ-PGA-Aln10-Phe in 1 M PB showed improved mechanical strength compared to those formed in 500 mM PB, while non-hydrophobically modified γ-PGA-Aln10 exhibited a reduction in mechanical performance (Figure 2j). At higher phosphate buffer (PB) concentrations, the formation of a star-shaped HAp layer, combined with different polymer configuration due to hydrophobic group incorporation, may enhance binding efficiency and improve mechanical performance [44, 45]. In contrast, the linear γ-PGA-Aln10 polymer may align more effectively with less sterically hindered particles, resulting in higher compressive strength under lower PB concentration. Based on the observed homogeneity and increased Young's modulus of γ-PGA-Aln10-Phe hydrogels in 1 M PB, this formula was selected and used for further stability and morphological analysis. To assess long-tern structural integrity, the stability of materials with and without hydrophobic modification in aqueous media was evaluated. The specific diameters of individual samples at different immersion times were measured and are summarized in Figure 2k. The non-conjugated γ-PGA-Aln10 hydrogel showed structural collapse after 24 h, while the hydrophobic conjugated dramatically improved stability. Higher Phe grafting degree was found to be critical for stability as Phe grafting degrees of 30% led to structural instability after 3 h, while grafting degree of 55% and 70% maintained structural integrity for up to 24 h (Figure 2l). Based on these results, γ-PGA-Aln10-Phe55 formed in 1 M PB with 1 wt% CaO_2 NPs was selected for subsequent studies.

Similarly to the γ-PGA-Aln10 oxygen-releasing hydrogel, the bubble effect on morphological structure of the γ-PGA-Aln10-Phe55 hydrogel was also examined. Figure 2m shows the macroscopic appearance of the hydrogel at 0 and 24 h, along with corresponding phase-contrast and SEM of cross-sectional images. These results confirmed the stabilizing effect of the hydrophobic domain, as no notable swelling was observed. Phase-contrast and SEM images at both time points showed no notable changes in bubble size within the gel, and CaO_2 NPs remained visible at both time points, as confirmed using elemental mapping (Figure 2n). Bubbling size from each analysis method was summarized in Figure 2o. The bubble size obtained from phase-contrast images showed a 1.1-fold increase after 24 h of incubation (61 μm to 70 μm), and the average pore size measured from SEM images showed 1.4-fold increase (0.66 μm to 0.93 μm). Although it shows a similar increasing trend compared with non-conjugated γ-PGA-Aln10 hydrogel, the hydrophobic Phe conjugation confirms long-term stability in aqueous conditions, making it suitable to use as the oxygen-releasing hydrogel for the construction of thick tissue scaffolds.

2.4 | Suppression of Bubble Formation: Catalase Mixing versus Coating

The general mixture of catalase with CaO_2 NPs and polymer solution for hydrogel formation is shown in Figure 3a. When catalase was mixed directly within the hydrogel, visible swelling could be clearly observed after leaving at room temperature for 1 min, however, the structure collapsed after 1 h incubation in aqueous solution. A photograph taken at 1 min after fabrication is shown in Figure 3b. The bubbling formation and position of catalase via phase contrast and fluorescence signal from FITC-catalase was observed using fluorescence microscopy as shown in Figure 3b(i,ii). Compared with the hydrogel without catalase (Figure 2m), the presence of catalase resulted in prominent swelling and noticeable bubble formation also visible in both images, suggesting active oxygen release throughout the hydrogel matrix. Similarly, SEM imaging of the same region (white box) shown in Figure 3b(iii) revealed porosity distributed across both the inner and outer regions of the hydrogel. This porous morphology is attributed to oxygen formation during gelation, as well as excess oxygen generated via catalase activity. Such excessive oxygen evolution is likely to disrupt the polymer network, leading to increased porosity, reduced structural integrity, and a more fragile hydrogel.

Coating efficiency and structural assessment of the catalase coating method was further evaluated (Figure 3c). The coating was performed at 4°C to minimize enzyme activity during the process. Coating efficiency was first evaluated by immersion in different concentrations of FITC-labeled catalase, specifically from 10 to 200 U/mL. As expected, after 1 h of coating, higher catalase concentrations were found to yield greater coating efficiency on the hydrogel surface, resulting in the highest fluorescence signal (Figure 3d). The effect of coating time was also evaluated. Using a constant catalase concentration of 200 U/mL, the fluorescence signal was observed at different time points, from 1 min up to 1 h. As shown in Figure 3e, fluorescence intensity increased approximately 10-fold after 10 min of immersion compared to the 1 min condition. Subsequently, the signal plateaued at

experiment ($n = 3$). For each experiment, at least three images were analyzed, with a minimum of 20 bubbles or pores quantified per condition using ImageJ. Two-tailed unpaired t-test was used for the analysis. Next, polymer with Phe conjugation, γ-PGA-Aln10-Phe, was further assessed for gelation ability and mechanical properties (j–o). (j) Young's modulus of hydrogels under different phosphate buffer concentrations (500 mM and 1 M) ($n = 3$ independent experiments). Data are analyzed using a two-tailed unpaired t-test. Stability assessment of fabricated hydrogels was evaluated through (k) changes in material diameter in aqueous media overtime ($n = 3$ independent experiments). (l) Representative images at each time point (scale bar = 5 mm). Structural analysis of 10% w/w γ-PGA-Aln10-Phe55 1 wt% CaO_2 NPs (1 M PB) oxygen-releasing hydrogel via (m) whole-gel, phase contrast, and SEM imaging of cross-sectioned fabricated gel. (n) SEM-EDS analysis at the yellow arrow position in the SEM image at 0 h and 24 h. (o) Bubble size distribution at 0 h and 24 h from phase contrast and SEM imaging. Data are summarized from three independent experiments ($n = 3$). At least three images were analyzed per each independent experiment, with a minimum of 20 bubbles or pores measures per image using ImageJ. Data are analyzed using a two-tailed unpaired t-test. Representative images from at least three independent experiments are shown.

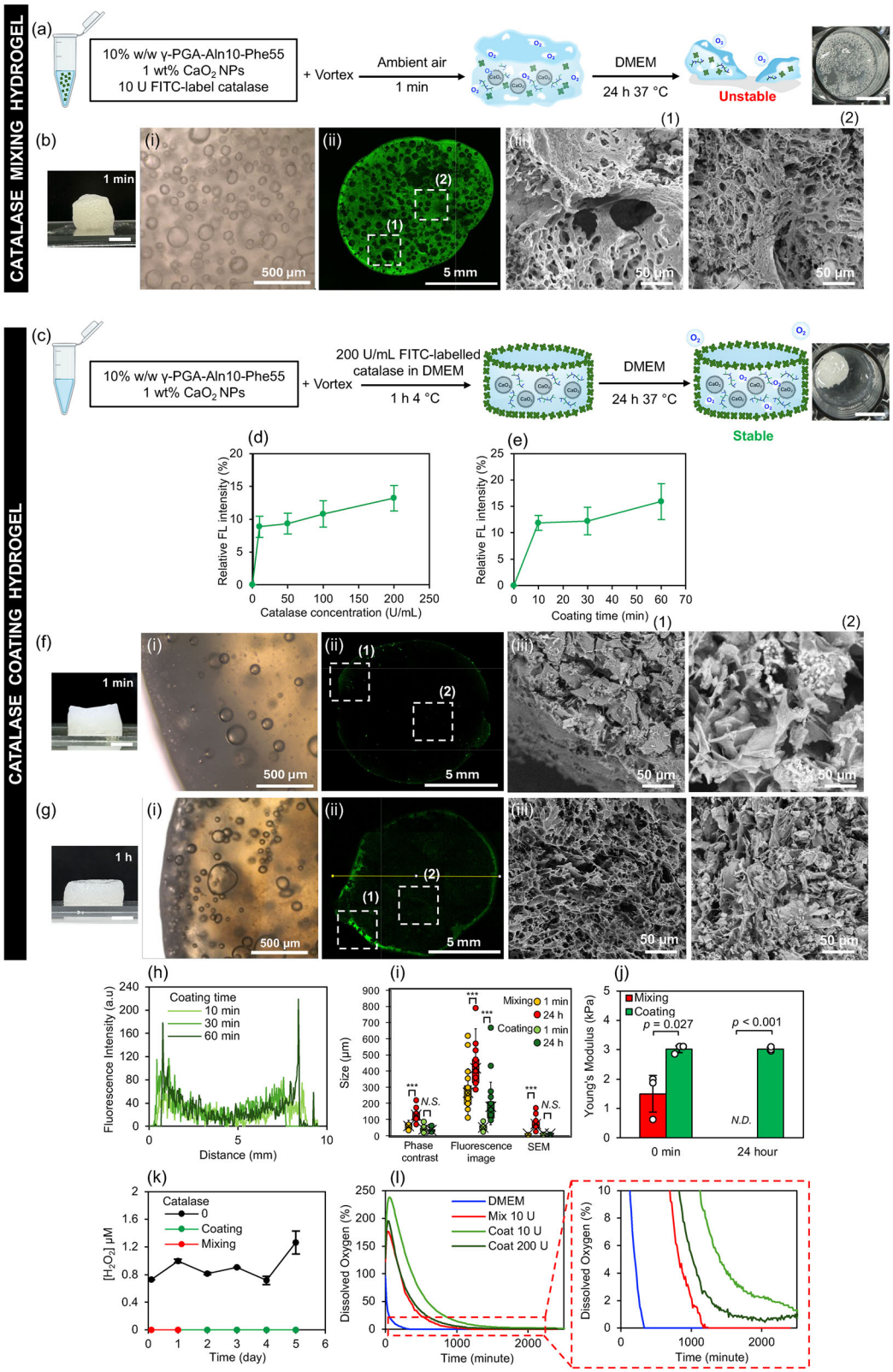

FIGURE 3 | Impact of the catalase incorporation method on bubble formation, hydrogel structure, and stability. (a) Schematic illustrating the fabrication procedure of incorporating of catalase via a direct mixing technique. Scale bar = 5 mm. (b) Representative image of the hydrogel after 1 min leaving at room temperature. Scale bar = 5 mm. Cross-sectioned samples were analyzed for bubble formation and catalase distribution using (i) phase-contrast imaging, (ii) fluorescence microscopy, and (iii) SEM. (c) Schematic illustrating the catalase coating technique developed in this study. Scale bar = 5 mm. (d) Coating efficiency quantified as relative fluorescence intensity at different catalase concentration, maintaining a 1 h coating time. (e) Relative fluorescence intensity as a function of coating time, maintaining catalase concentration of 200 U/mL ($n = 3$ independent experiments). Representative images of hydrogels after (f) 1 min and (g) 1 h of catalase coating. Scale bar = 5 mm. The cross-sectioned hydrogels were similarly examined for bubble

30 min and showed only a slight increase at 1 h. Based on these findings, hydrogels were subsequently immersed in the catalase-containing solution at a concentration of 200 U/mL for 1 h. Notably, this formulation was confirmed to maintain hydrogel structural stability in aqueous solution for over 24 h.

For comparison with the direct mixing technique as discussed earlier, the same evaluation protocol was applied. Initially, the fabricated gel coated with catalase for 1 min did not show notable swelling compared to the mixing technique (Figure 3f). Furthermore, phase-contrast imaging also showed only slight bubble formation at the periphery of the hydrogel (Figure 3f(i)). Consistent with this observation, the fluorescence signal in Figure 3f(ii) confirmed the presence of catalase on the hydrogel surface. However, due to the short immersion time, only a partial signal could be observed. SEM images taken at two different positions, specifically, the outer and inner parts of the coated hydrogel revealed the presence of CaO_2 NPs in both regions, suggesting that the coating process did not interrupt CaO_2 within the hydrogel structure (Figure 3f(iii)). Next, 1 h coating was further evaluated. A hydrogel image capture after 1 h immersion is shown in Figure 3g, where no distinct swelling was observed. However, a small bubble formation around the periphery of the hydrogel was noticeably increased compared to 1 min coating (Figure 3g(i)). This could have resulted from the enzymatic reaction of catalase that happens on the surface of the hydrogel. This hypothesis was confirmed by the increasing strength of the fluorescence signal near the gel surface (Figure 3g(ii)). It is once again confirmed that longer coating time allows for higher coating efficiency, resulting in greater enzymatic activity predominantly at the hydrogel's surface. This is supported by SEM images, which show a distinct morphology at the surface area compared to the inner region (Figure 3g(iii)). The penetration ability of catalase into the hydrogel under different coating times was also evaluated using fluorescence intensity mapping (represented by the yellow line across the hydrogel). As demonstrated in the fluorescence mapping in Figure 3h, a longer coating time resulted in a higher fluorescence signal. For the 1 h coating time, the signal was clearly observed predominantly around 1 mm from the outer surface before gradually declining toward the inner regions. In the same region, the 10 min and 30 min conditions showed progressively lower fluorescence signals. This result further supports the assertion that enzymatic reaction is concentrated near the hydrogel surface, potentially preserving embedded CaO_2 NPs and extending their functional lifespan.

Bubble size from the catalase-mixing and coating techniques was comprehensively analyzed and summarized using phase contrast, fluorescence, and SEM analysis (Figure 3i). Because catalase-mixed hydrogels rapidly collapse in aqueous solution, therefore, all samples were maintained under ambient air for 1 min and 24 h after catalase incorporation (Figure S4). Catalase-coated conditions were coated for 1 h and subsequently left in ambient air for 1 min or 24 h before further analysis. Quantitative analysis showed that the mixing method caused a pronounced increase in bubble size and porosity after 24 h, with 2.1-, 1.6-, and 6.6-fold increases across the three imaging techniques. In contrast, the coating method showed only modest changes of 0.84-, 3.5-, and 0.92-fold, respectively. Direct comparing between the two techniques after 24 h demonstrated that the coating approach yielded 3.8-, 2.3-, and 5.9-fold smaller in bubble size than the mixing technique. These results indicate that surface immobilization of catalase more effectively preserves hydrogel structural integrity than the mixing method. This preservation may prolong the oxygen-releasing activity of CaO_2 NPs and minimize burst release caused by rapid catalase activity. Taken together, these results confirm the surface-localized coating of catalase demonstrating its effectiveness in preserving hydrogel morphology, potentially contributing to prolonged structural stability over time.

Following the confirmation of catalase coating efficiency, the mechanical properties were further evaluated. Hydrogels prepared using catalase mixing or surface-coating methods, with equivalent catalase content, were freshly fabricated and immersed in serum- and phenol red-free DMEM prior to further analysis. After mixing or coating of catalase, compression testing was performed immediately to assess the initial mechanical integrity of each method. As shown in Figure 3j, the Young's modulus of the coating method was 3 kPa, which was 2-fold higher than the mixing method. However, after 24 h of immersion, the catalase-mixed method had completely degraded, preventing further mechanical assessment. In contrast, the coated samples retained their structure and preserved their mechanical strength at 3 kPa. These findings align with earlier morphological observations, where the mixing method resulted in pronounced porosity throughout the gel immediately after fabrication, compromising structural integrity.

2.5 | Enzymatic Activity and Cytotoxicity Assessment

Next, the release of H_2O_2 was measured by collecting the incubation medium at a defined time point. Owing to the enhanced structural stability of the coated hydrogel, measurements could

morphology using (i) phase-contrast imaging, (ii) fluorescence microscopy, and (iii) SEM. (h) Fluorescence intensity mapping of different coating times across a cross-sectioned hydrogel (mapping area indicated by the yellow line), maintaining catalase concentration of 200 U/mL. (i) Summary of bubble size quantified from phase-contrast image, fluorescence, and SEM image. Catalase-mixing condition, hydrogels were analyzed after incorporating with 10 U catalase and left in ambient air for 1 min or 24 h, as samples collapsed upon immersion in aqueous solution. While catalase-coating condition, hydrogels were immersed in catalase solution for 1 h before being exposed to ambient air for 1 min or 24 h prior image analysis. Data are summarized from three independent experiments ($n = 3$). For each experiment, at least three images were analyzed, with a minimum of 20 bubbles or pores quantified per condition using ImageJ. Independent samples were used at each time point and analyzed using a two-tailed unpaired t-test. (j) Young's modulus of hydrogels incorporating catalase via mixing or coating methods, measured before and after 24 h immersion in aqueous solution (n = 3 independent experiments). Data analyzed using two-tailed unpaired t-test. (k) H_2O_2 release and (l) O_2 release profile under hypoxic conditions over time ($n = 3$ independent experiments). Data represent mean ± SD. $^{*}p < 0.05$, $^{**}p < 0.01$, $^{***}p < 0.001$. Representative images are from at least three independent experiments.

be consistently performed over 5 days, while the mixed hydrogel degraded within 1 day, limiting only a single time point. Showing in Figure 3k, both the mixing and coating strategies effectively suppressed H_2O_2 as no detectable levels were found in the respective medium. Conversely, the control hydrogel without the presence of catalase exhibited continued H_2O_2 release of 1 μM overtime, which could lead to oxidative stress and affect the cell viability due to reactive oxygen species (ROS) generation [46, 47]. These findings confirm that the coating method prolongs hydrogel stability while sustaining H_2O_2 suppression over time. Oxygen release profile of the hydrogel was assessed (Figure 3l). Control hydrogel without catalase released oxygen for up to 24 h before the oxygen level dropped to 0%. The hydrogel mixed with catalase released oxygen for approximately 20 h before complete depletion. However, the catalase-coated hydrogel demonstrated sustained oxygen release for up to 3 days. These results align with the structural stability and H_2O_2 measurements, which indicated that the mixing method led to faster degradation in aqueous media. Interestingly, catalase concentration during coating influenced the initial oxygen release profile. A pronounced burst was observed within the first hour for hydrogels coated with 10 U/mL catalase, whereas 200 U/mL exhibited a more gradual and attenuated peak. This difference may reflect early surface reactions during the coating process, as more catalase may have adhered at higher concentrations, consistent with the fluorescence data in Figure 3f. A lower initial oxygen spike, as seen with 200 U/mL, could be advantageous for cell viability by avoiding burst release of oxygen and the associated oxidative stress [48]. Collectively, these results demonstrate that strategic catalase positioning not only suppresses H_2O_2 accumulation but also modulates oxygen release kinetics, validating its potential as a controlled oxygen-releasing strategy. However, compared to other reports where oxygen release was sustained for up to 10 days or even 1 month [49, 50], a shorter release duration in this study is expected. This is due to the use of CaO_2 NPs as the primary crosslinking site in hydrogel fabrication, without additional crosslinking sources.

Prior to scaffold construction, the cytotoxicity of the material was first evaluated under hypoxic conditions (5% CO_2, $O_2 < 0.1\%$, 37°C). Normal human dermal fibroblasts (NHDFs) were seeded with or without the presence of catalase-coated hydrogels placed in cell culture inserts (Figure S5a). After 3 days, phase-contrast images showed enhanced cell spreading and a 1.8-fold increase in cell number in the catalase-coated condition compared with controls (Figure S5b,c). Because H_2O_2 is a by-product of CaO_2 decomposition and is known to induce oxidative stress and apoptosis [51, 52], intracellular ROS were quantified by Detection Cell-Based Assay Kit (Figure S6a,b). ROS fluorescence in absence of catalase were approximately 8-fold higher than in catalase-coated samples. In contrast, catalase coated samples exhibited only 1% of the ROS signal relative to controls, indicating effective suppression of oxidative stress. Consistent with H_2O_2 release data, these findings demonstrate that catalase coating mitigates cytotoxic by-products and ensures material safety for thick scaffold fabrication.

2.6 | Cell Response to Catalase-Coated Oxygen-Releasing Hydrogel Scaffolds in a Hypoxic Environment

Millimeter-scale scaffold embedded with a catalase-coated oxygen-releasing hydrogel was further fabricated (Figure 4a). NHDFs were used to evaluate cell viability and behavior within scaffolds containing fibrin gel alone and hydrogel coated with 0, and 200 U/mL of catalase. To assess the impact of catalase-coated oxygen-releasing hydrogels on cell behavior, the constructs were cultured under hypoxic conditions for up to 10 days. The total DNA content at days 5 and 10 of culture was expressed as a percentage relative to the initial DNA content on day 0 of culture as shown in Figure 4b. After 5 days of culture, the relative DNA content increased to 115%, 133%, and 150% for the fibrin gel alone, 0 U/mL, and 200 U/mL catalase-coated hydrogel, respectively. These values further increased by day 10 to 157%, 145%, and 172%, respectively. Interestingly, even in the fibrin gel alone, DNA content increased over time, likely due to cellular adaptation to hypoxia and greater space for cells to continue to proliferate. Under low oxygen conditions, cells tend to shift their metabolism toward glycolysis, thereby maintaining ATP production to support survival and proliferation [53]. In contrast, oxygen-releasing hydrogels, especially with a catalase coating, supported enhanced cell proliferation rate, despite occupying physical space within the scaffold that may modestly limit cell expansion. This suggests that oxygen availability, rather than space alone, plays a dominant role in sustaining cell growth under hypoxic stress. While hydrogels without catalase also supported increased DNA content, the growth rate began to plateau by day 10, showing only a 1.09-fold increase compared to a 1.15-fold increase with catalase-coated hydrogels. This difference suggests that gradual accumulation of H_2O_2 in the absence of catalase may inhibit long-term cell proliferation.

The viability of cells within the scaffold was also assessed via Live/Dead staining (Figure 4c,d), focusing on the scaffold's upper region where hydrogel exposure was most direct. Surface imaging revealed minimal cell death in control samples, likely due to higher nutrient accessibility. In contrast, catalase-free hydrogels showed elevated cell death, consistent with increased ROS and reduced viability. Quantification confirmed that catalase-coated hydrogels preserved 95% cell survival, compared to just 47% without coating (Figure 4e). Cytoskeletal staining (Figure S7) revealed that cells exposed to catalase-coated hydrogels exhibited elongated morphology and well-organized F-actin, comparable to controls. This spread phenotype is associated with enhanced adhesion, cytoskeletal tension, and mechanotransduction, factors known to promote proliferation and migration. In contrast, cells without catalase appeared rounded, indicative of poor substrate interaction and reduced viability, which can impair both proliferative capacity and motility. These findings confirm the strong potential of catalase coated oxygen-releasing hydrogels to support both cell proliferation and viability under hypoxic conditions.

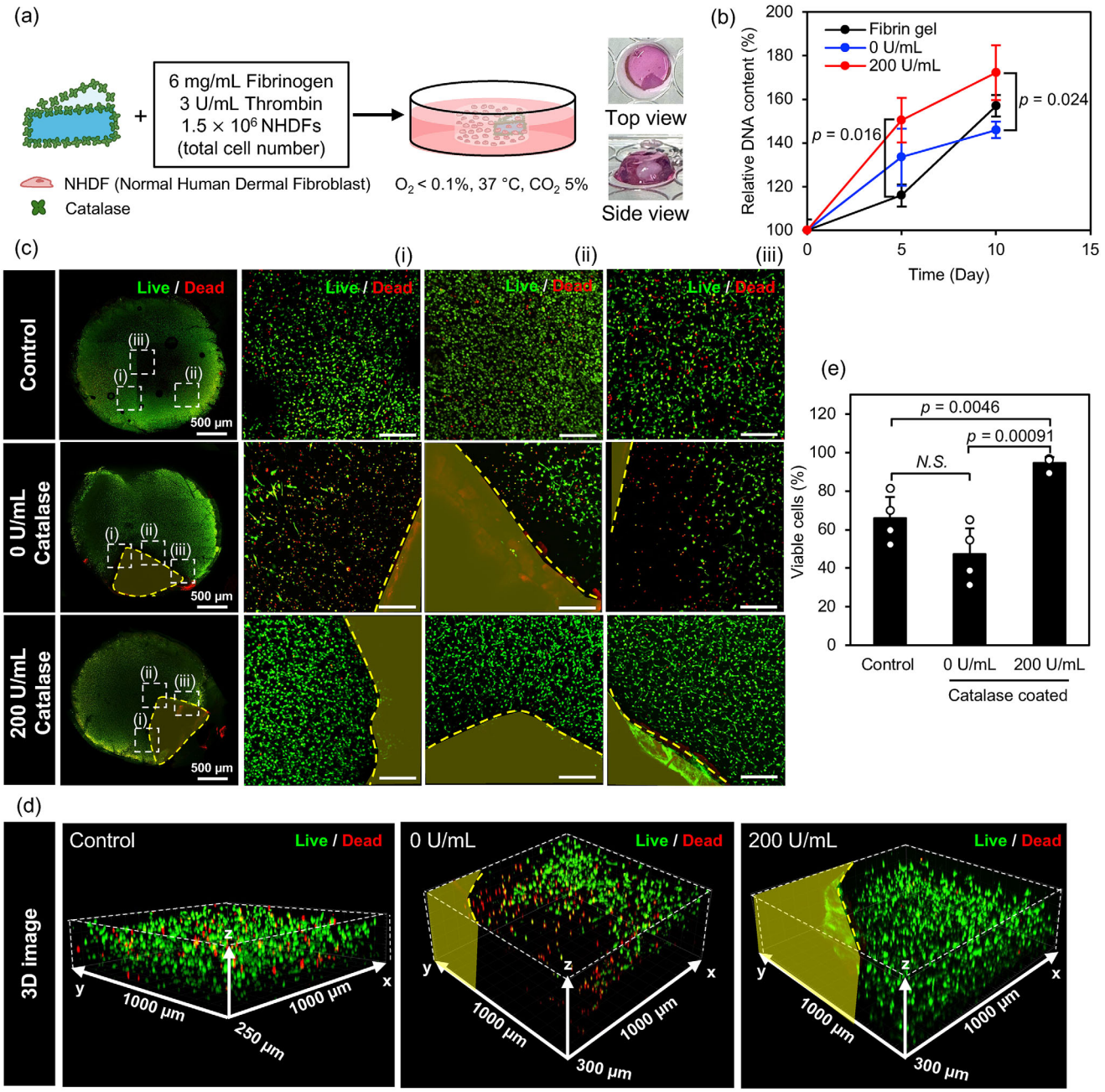

FIGURE 4 | 3D tissue constructs for evaluating cell viability under hypoxic conditions. (a) Schematic illustration of the fabrication of the fibrin scaffold NHDFs that were incorporated into the fibrin hydrogel, followed by the embedding of the catalase-coated quarter hydrogel The entire construct was then cultured in a 6-well plate under hypoxia conditions, 37°C, and 5% CO_2 for 5 days. (b) Relative DNA content of scaffolds collected at different time points, expressed as a percentage of initial DNA content on day 0 ($n = 3$ independent experiments). Data analyzed by one-way ANOVA with Tukey's post-hoc test. (c) Representative Live/Dead fluorescence images of fibrin gels after 5 days of culture. (Z-stack projections showing images from different positions within each sample. Scale bar = 500 μm. (d) 3D fluorescence reconstructions of representative regions from each condition. (e) Quantitative analysis of Live/Dead images for cell viability within scaffolds after 5 days of culture, data are calculated with respect to the total nuclei. Data are presented as mean ± SD from four independent experiments ($n = 4$). For each experiment, values were averaged from three images. Statistical analysis was performed using one-way ANOVA with Tukey's post-hoc test. Representative images are from at least three independent experiments.

2.7 | Fabrication of a Centimeter-Scale 3D Tissue

To evaluate the potential of the catalase-coating strategy proposed in this study for supporting cell viability in thick scaffolds, we fabricated centimeter-scale fibrin scaffolds using a sandwich method. Each scaffold encapsulated a total of 15×10^6 NHDFs and incorporated the oxygen-releasing hydrogels either with or without the catalase coating. The resulting scaffold, shown in Figure 5a, was 1 cm in diameter and 1.5 cm in height, with the hydrogel positioned at the center. The scaffolds were subsequently cultured for 5 days under hypoxic conditions. A light-sheet fluorescence microscope (LSFM) was used to capture whole-scaffold images (Figure 5b, Supporting Video 2a–c), where f-actin and nuclei staining suggested a uniform distribution of

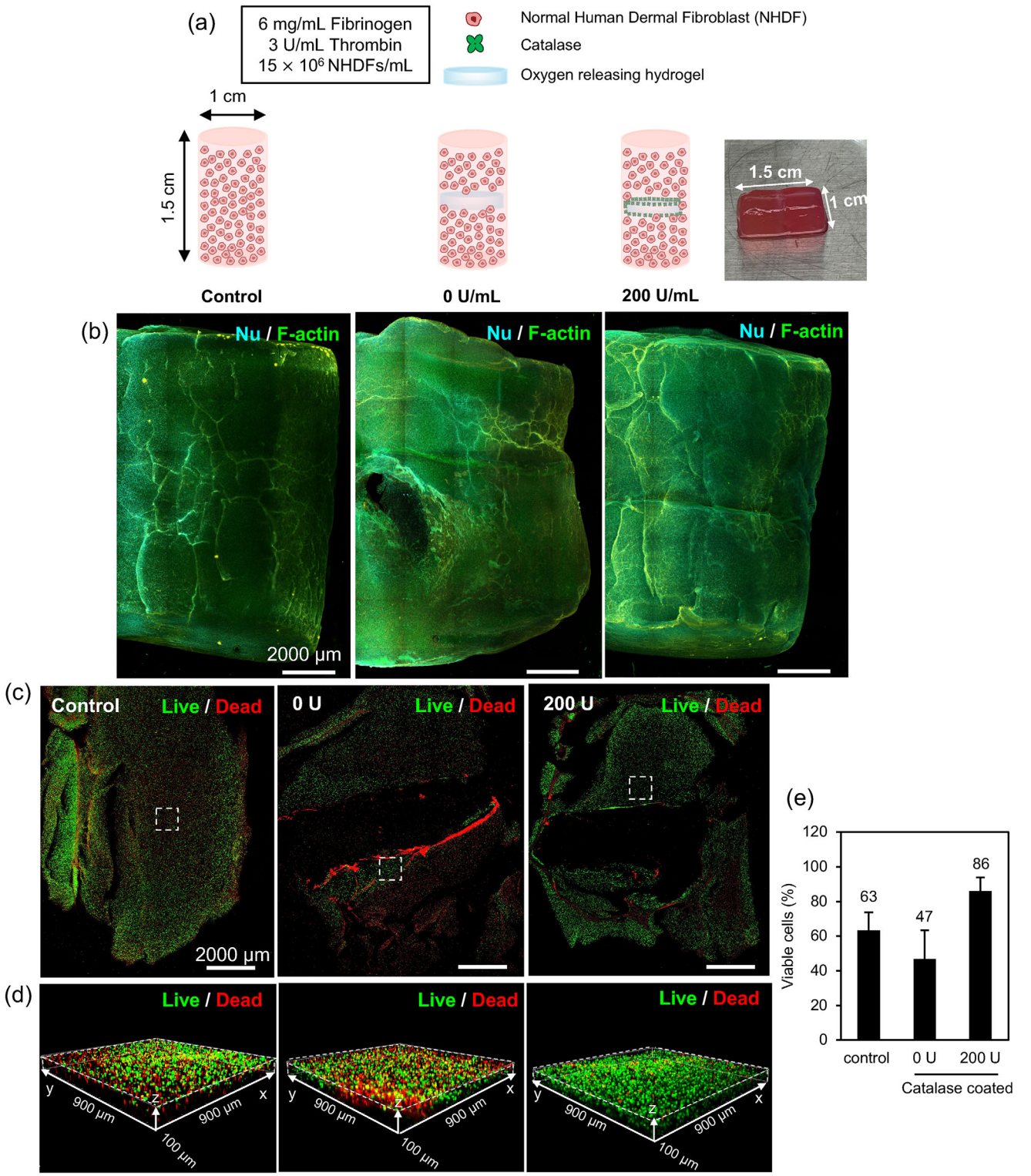

FIGURE 5 | Fabrication of centimeter-scale fibrin gel scaffolds. (a) Schematic illustration of the centimeter-scale scaffolds for cell culture. The three conditions included scaffold without oxygen-releasing hydrogel (control), with non-catalase-coated oxygen-releasing hydrogel, and with catalase-coated oxygen-releasing hydrogel. Constructs were cultured under hypoxic conditions (O_2 < 0.1%), 37°C, 5% CO_2 for 5 days. (b) Light-sheet microscopy image of the entire scaffold showing immunofluorescence staining of nuclei (cyan) and F-actin (green), used to evaluate cell distribution and localization throughout the construct. Scale bar = 2000 μm. (c) Live/Dead images of cross-sectioned scaffolds. Scale bar = 2000 μm. (d) 3D fluorescence reconstructions of representative regions from each condition. (e) Quantification of cell viability from Live/Dead staining, calculated with respect to the nuclei (n = 15 independent areas), data are presented as mean ± SD within a single representative experiment.

cells throughout the construct. To further assess cell viability, scaffolds from each condition were bisected and stained using Live/Dead assay (Figure 5c). In the control sample, noticeable cell death was observed in the inner regions of the scaffold (Figure 5d), consistent with limited nutrient and oxygen diffusion [54]. Embedding oxygen-releasing hydrogels improved oxygen availability, but in the absence of catalase, excessive H_2O_2 accumulation led to widespread cytotoxicity. In contrast, scaffolds incorporating catalase-coated hydrogels showed a good distribution of viable cells, confirming that enzymatic decomposition of H_2O_2 not only mitigated oxidative stress but also enabled deeper oxygen release for supporting cell survival within thick, hypoxic scaffolds (Figure S8).

Quantitative analysis of Live/Dead cells was then conducted from 10× magnification images throughout the scaffold (Figure S9 and Figure 5e). Quantitative image analysis performed on a representative scaffold demonstrated a trend similar to that observed in the millimeter-sized scaffolds. Under the complete absence of oxygen, the control scaffold resulted in 63% viable cells. Viability was further reduced to 47% with the incorporation of the non-catalase-coated hydrogel. Conversely, our catalase-coated material showed up to 86% viable cells, which is 1.3- and 1.8-fold higher than the control and the non-catalase-coated conditions, respectively. To further assess hypoxia distribution within the thick scaffold, a phosphorescent and cell-permeable hypoxia probe (LOX-1) was used [55]. Strong LOX-1 signals were detected throughout the control scaffold at Day 1, as expected due to the exposure of embedded cells to low oxygen levels (Figure S10a). In contrast, scaffolds containing the catalase-coated oxygen-releasing hydrogel exhibited lower LOX-1 phosphorescence intensity levels at the same time point. Although a slight increase in the LOX-1 signals was detected on Day 3, the scaffold's inner region continued to display lower fluorescence intensity compared with the control group (Figure S10b,c). Quantitative analysis of higher-magnification images showed approximately 30% and 48% LOX-1 positive cells in scaffolds containing the catalase-coated oxygen-releasing hydrogel at Day 1 and Day 3, respectively, whereas the control scaffold exhibited approximately 94% LOX-1-positive cells at Day 1 (Figure S10d,e). This trend was consistent with the oxygen-release profile of the material, which showed higher oxygen generation during the initial stage followed by a gradual decrease over time. These findings suggest that the catalase-coated oxygen-releasing hydrogel could provide localized oxygen to centimeter-scale cell-laden scaffolds in a hypoxic environment, supporting and sustaining the survival of embedded cells.

2.8 | Effect of Catalase-Coated Oxygen-Releasing Hydrogel on Cell Survival and Neuronal Differentiation of Human Neural Stem Cells in a Severe Hypoxia Environment

2.8.1 | Cell Metabolic Activity and Viability

After confirmation of its feasibility for centimeter-scale scaffold fabrication, we further investigated the performance of the system using a cell type more sensitive to oxygen stimulus, specifically human neural stem cells (hNSCs) cultured under neuronal differentiation conditions. The study was designed to evaluate the potential of the oxygen-releasing hydrogel to sustain cell viability and neuronal differentiation of hNSC under severe hypoxic conditions, inspired by the translational potential of this system for NSC transplantation therapies targeting ischemic brain injuries (Figure 6a). The cytocompatibility of the material toward hNSCs was first evaluated. Results demonstrated less than 10% of cytotoxicity in the LDH assay and approximately 70% of cell metabolic activity retention in the resazurin reduction assay, indicating that the oxygen-releasing hydrogel is non-cytotoxic toward hNSCs, according to ISO 10993–5 criteria (Figure S11b,c) [56]. The oxygen content within the modified fibrin gel construct was then validated, where the fibrin-embedded oxygen-releasing hydrogel exhibited sustained oxygen release for up to 30 h, compared to approximately 15 h for the non-embedded group (Figure 6b). Subsequently, hNSC-laden fibrin gels were cultured under neuronal differentiation and severe hypoxic conditions (O_2< 0.1%), and cell metabolic activity was longitudinally monitored (Figure 6c). Both groups exhibited comparable metabolic activity profiles throughout the culture period. Although intermittent exposure to ambient air (~21% oxygen) during media exchange may have partially reduced the differences between groups, the observed trend remained consistent with previous reports describing the metabolic adaptation of cells exposed to sustained hypoxic conditions [57, 58].

Oxygen-releasing hydrogels supported cell survival in severe hypoxic environment, as shown by the Live/Dead assay and viable cell quantification, respectively (Figure 6d,e). Live/dead staining of cells at Day 1 and Day 12 of differentiation demonstrated pronounced dead cell accumulation within the inner region of the fibrin gel in the absence of the oxygen-releasing hydrogel, whereas lower dead cell staining was observed within the inner region in the presence of the hydrogel. Subsequent analysis of the projected CLSM stacks revealed higher live cell percentages in the presence of the oxygen-releasing hydrogel, showing 83% and 71% viability at Day 1 and Day 12, respectively, compared to 62% and 38% in the absence of the hydrogel. Similarly, quantification of viable cells using the trypan blue dye exclusion assay after cell isolation from the cell-matrix constructs revealed 1.5-, 1.2-, 1.3-, and 1.4-fold increases at Day 1, 3, 5, and 12, respectively, presenting higher numbers of viable cells in fibrin gels embedded oxygen-releasing hydrogel, as compared to the control group (Figure 6f). Total DNA quantification showed a trend for an increase in DNA content over the culture period for both conditions, and higher DNA content at Day 12 of culture in the control condition than in fibrin gels containing the oxygen-releasing hydrogel (Figure 6g). This increase may be associated with hypoxia-induced metabolic adaptation and the maintenance of hNSC self-renewal, as the native NSC niche is physiologically hypoxic [59, 60]. In fact, the formation of cellular spheroids resembling neurospheres observed after 8 days of cell culture suggests that hNSC + proliferation continued throughout the culture period. Nevertheless, despite the higher DNA content observed in the control group, sufficient oxygen availability remains critical for maintaining long-term cell survival and supporting neuronal differentiation [36, 61, 62]. Although the oxygen-releasing hydrogel sustained oxygen release for only approximately 2 days, these findings suggest that oxygen release supplementation during the initial culture stage may play an important role in preserving cell viability and influencing subsequent cellular behavior under prolonged severely hypoxic conditions. As such, the influence

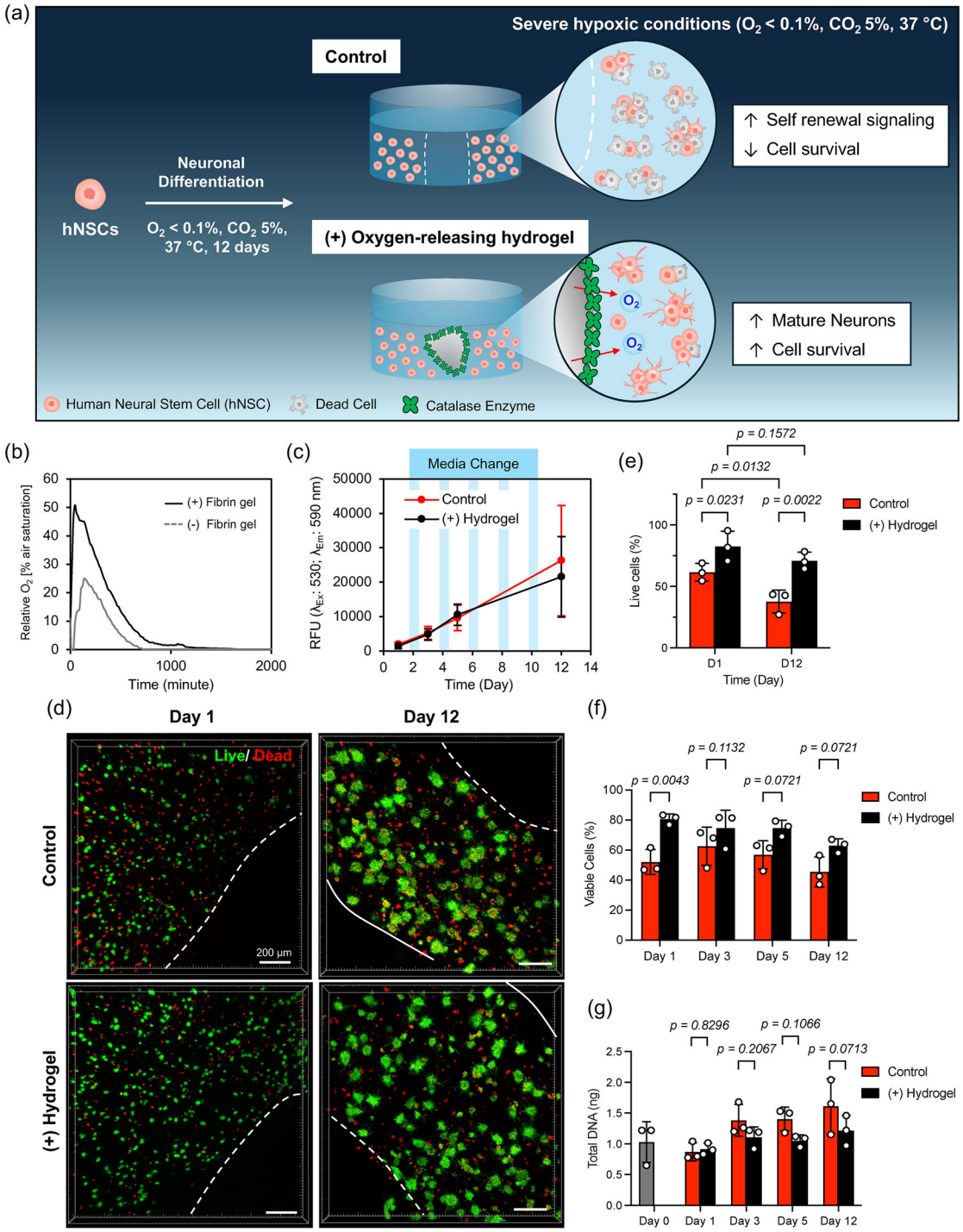

FIGURE 6 | 3D culture of human neural stem cells (hNSCs) in fibrin gel under severely hypoxic ($O_2 < 0.1\%$) and neuronal differentiation conditions, in the absence or presence of catalase-coated oxygen-releasing hydrogel. (a) Schematic illustration of the 3D-hNSCs-fibrin gel construct. (b) O_2 content within fibrin gel (average of $n = 3$ independent experiments). (c) Cell metabolic activity as a function of culture time, determined using the resazurin assay ($n = 3$ independent experiments). (d) Representative 2D projections of CLSM image stacks of the cell-laden fibrin gels showing viable/dead cells around the inner region of the fibrin gel. Scale bar = 200 µm. (e) Cell viability quantification, as determined by image analysis of CLSM 2D projections (mean ± SD, $n = 3$ independent experiments). (f) Percentage of viable cells quantified using the Trypan blue dye exclusion method and (g) Total DNA, assessed using a Qubit dsDNA Assay kit, expressed as Total DNA (ng). Both data are summarized per fibrin gel ($n = 3$ independent experiments). Statistical analysis was performed using two-way ANOVA followed by the Holm-Šídák multiple comparison test. (h) Distribution of mature neurons after 12 days of neuronal differentiation, assessed by immunofluorescence labelling of MAP2 (red) and nuclei counterstaining (blue). Scale bar = 300 µm and 100 µm. (i) Quantitative cell expression of βIII-Tubulin (developing and mature neurons) and MAP2 (mature neurons) at day 12, as determined by flow cytometry analysis of cells pooled from 10 replicate fibrin gels ($n = 1$ independent experiment). (j) Average volume of cellular spheroids (neurospheres) at day 12 of differentiation ($n = 3$ independent experiments). (k) Maximal neurite branching level, (l) average number of neurites sprouting per neurosphere, and (m) maximal neurite length at day 12 of culture. Data are presented as mean ± SD ($n = 3$ independent experiments). Statistical analysis was performed using the unpaired Mann-Whitney test.

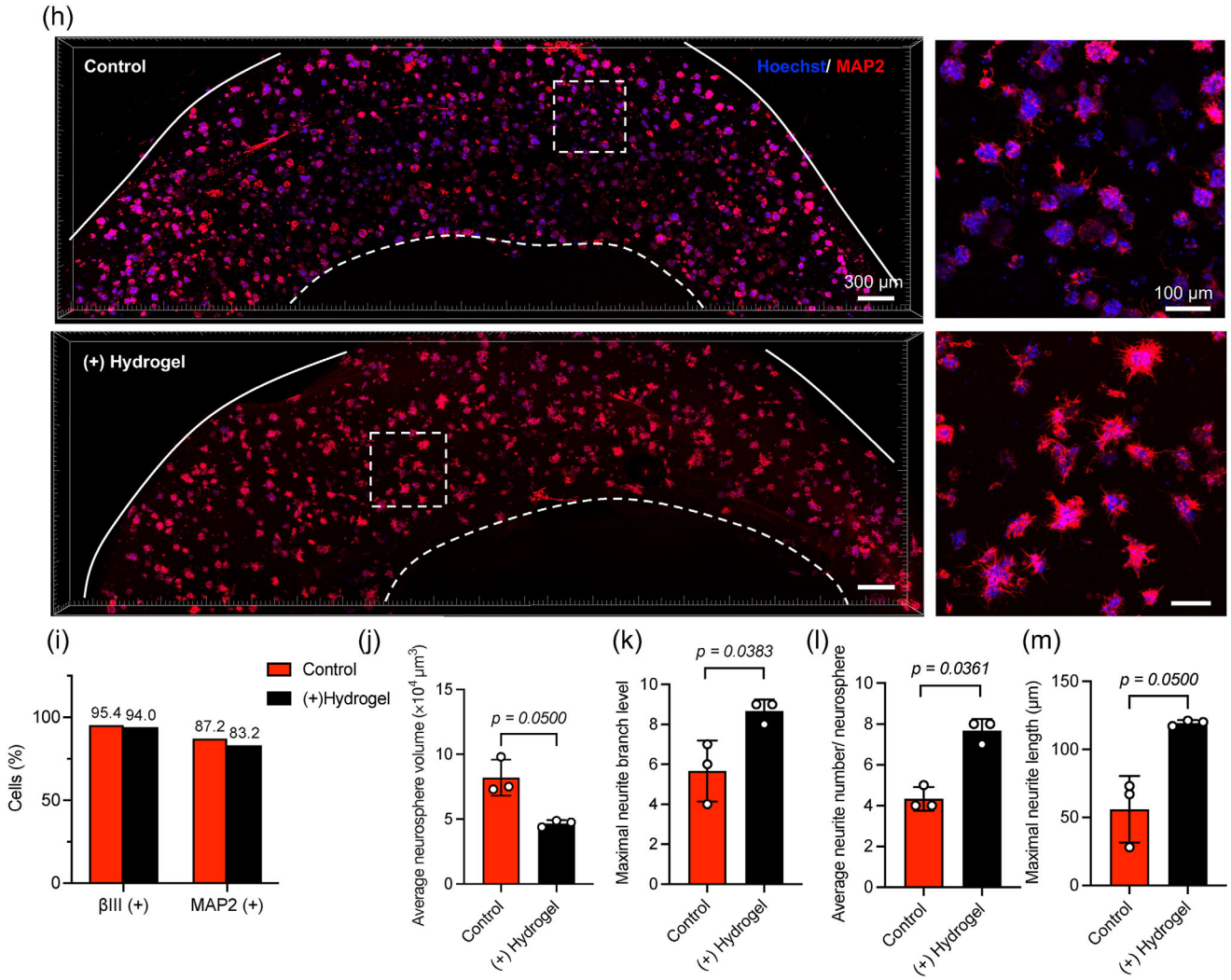

FIGURE 6 | (Continued)

of the oxygen-releasing hydrogel on neuronal differentiation and maturation was subsequently addressed.

2.8.2 | Oxygen Support for Neuronal Maturation Under Severe Hypoxic Conditions

Transplantation of NSCs has been considered a promising therapeutic strategy for ischemic stroke due to their neuroprotective effects and ability to replace lost neurons [39]. However, post-transplantation cell survival and efficient differentiation into mature neurons remains a major challenge [63]. Previous studies have reported that transplanted NSCs often preferentially differentiate into astrocytes, while neuronal differentiation after stroke remains very limited [64, 65]. In this study, to evaluate the influence of the oxygen-releasing hydrogel on neuronal differentiation and maturation under severe hypoxic conditions, we performed immunofluorescence labelling of Nestin (neural stem/progenitor cells), βIII-Tubulin (developing and mature neurons), and MAP2 (mature neurons marker), after 12 days of differentiation culture. Projected CLSM stacked images of Nestin and βIII-Tubulin double staining showed comparable marker expression between both groups (Figure S13a,b). However, βIII-Tubulin staining in the presence of the oxygen-releasing hydrogel exhibited more pronounced neurite extension from neurospheres compared to the control group, as highlighted by the white arrows in the images. A similar trend was observed in samples processed for MAP2 staining (Figure 6h). Consistent with the imaging results, flow cytometry studies revealed more than 80% of cells expressing both βIII-Tubulin and MAP2 in both groups (Figure 6i), as expected at this time point of neuronal differentiation culture [66, 67].

Interestingly, distinct differences in the morphology of cellular spheroids were observed between the two groups, particularly in terms of neurosphere size and neurite extension. hNSCs cultured in the presence of the oxygen-releasing hydrogel exhibited an approximately 1.8-fold smaller neurosphere volume compared to the control group (Figure 6j). This result aligns with the higher DNA content found in the control group (Figure 6g), where the oxygen-deficient environment possibly promoted hNSC proliferation and the formation of larger neurospheres. Larger neurospheres may be associated with increased nutrient and oxygen limitations within the inner region, potentially affecting cell survival and neuronal maturation [68]. Enhanced of neurite outgrowth was observed in the oxygen-releasing hydrogel group,

which showed 1.5-, 1.8-, and 2.1-fold higher maximal neurite branch level, average number of neurites per neurosphere, and maximal neurite length, respectively (Figure 6k,m). The increased neurite complexity and branching indicate enhanced neuronal maturation and structural development, both of which are essential characteristics for neuronal connectivity and functional neural network formation. Altogether, these findings suggest that our material can support hNSC mature neuronal differentiation under severe hypoxic conditions.

3 | Conclusion

In this study, we developed a rapid, selective, and biocompatible strategy for constructing oxygen-releasing hydrogels through the interaction between a γ-PGA-Aln-based polymer and CaO_2 NPs together with catalase-coating strategies on the hydrogel surface to minimize bubble formation within its structure. The system integrates chemical precision with structural robustness, enabling stable oxygen delivery while minimizing H_2O_2 accumulation and bubble-induced disruption. By localizing catalase activity at the hydrogel surface, the design achieved sustained oxygen generation under hypoxic conditions and preserved mechanical integrity across multiple scales. This points to the potential role of spatial enzyme localization in regulating oxygen release dynamics and material stability. Along with pointing to the potential role of the spatial enzyme localization in regulating oxygen release dynamics and preserving mechanical integrity, this study has proven these materials' cytocompatibility toward NHDFs and ability to promote cell survival when applied to thick cell-laden scaffolds.

In addition, this study addressed the potential of the catalase-coated oxygen-releasing hydrogels to support cell survival and neuronal differentiation of hNSCs in oxygen-deprived environments (O_2< 0.1%). Although no impact was observed at the level of neuronal marker expression in the absence or presence of the oxygen-releasing hydrogel, early oxygen supplementation significantly enhanced hNSCs survival and neuronal structural complexity, the latter evidenced by increased neurite extension and branching. These findings suggest that oxygen availability during the early stages of hNSC neuronal differentiation impacts neuronal maturation, which is a key aspect in neuronal replacement therapies. In summary, this work provides a proof-of-concept for the use of catalase-coated oxygen-releasing biomaterials as supportive platforms for oxygen supply to thick tissue-engineered constructs for application in severe oxygen-limited environments.

4 | Experimental Section

4.1 | Materials

Polyethylene glycol 200 (PEG200), disodium hydrogenphosphate (CAS RN: 7558-79-4), sodium dihydrogenphosphate (CAS RN: 7558-80-7), poly-(γ-glutamic acid) sodium salt (γ-PGA, Mw = 550 000 kDa), and phosphate buffer saline (D-PBS) were purchased from FUJIFILM Wako Pure Chemical Corporation, Osaka, Japan. Hydrogen Peroxide (35%) and ammonia Solution (28%) was purchased from Kishida Chemical Co., Ltd. (Japan). Alendronic acid (Aln) and ethyl-L-phenylalaninate hydrochloride (Phe) were purchased from Tokyo Chemical Industry Co., Ltd., Tokyo, Japan. The 4-(4,6-dimethoxy-1,3,5-triazin-2-yl)-4-methylmorpholinium chloride n-hydrate (DMTMM, 97.5%) was purchased from Watanabe Chemical, Japan. Sodium hydrogen carbonate ($NaHCO_3$) was purchased from Nacalai tesque. Dialysis tube (MWCO 12 000 ~ 14 000 kDa) was picked up from Fisher band. Deuterium oxide (99% atom % D). Calcium peroxide (CaO_2) (particle size < 200 mesh (74 μm)), catalase (from bovine liver, 2000 ~ 5000 U/mg), fibrinogen (from bovine plasma Type I-S, 65 ~ 85% protein), and thrombin (from bovine plasma 40 ~ 300 NIH units/mg protein) were purchased from Sigma-Aldrich. Fetal bovine serum (FBS) (10270), antibiotics (50 U/mL penicillin and 50 μg/mL streptomycin), and 4',6-diamidino-2-phenylindole (DAPI) were purchased from Thermo Fisher Scientific (MA). Normal human dermal fibroblasts (NHDF, CC-2509) were purchased from LONZA (Basel, Switzerland).

4.2 | Synthesis and Characterization of Calcium Peroxide Nanoparticles (CaO_2 NPs)

The synthesis of CaO_2 NPs was prepared as reported from Hu et al. and Tomioka et al. [69, 70]. based on the hydrolysis precipitation method, using the equation

$$CaCl_2 + H_2O_2 \rightarrow CaO_2 + 2HCl$$

$$2HCl + 2HN_3 \rightarrow 2NH_4\,Cl$$

The reaction was conducted with slight modifications. Briefly, 0.9 M (or 3 mg) of $CaCl_2$ was dissolved in 3 mL of water, followed by the addition of 12 mL of PEG-200. The solution was continuously stirred at 600 rpm in an ice bath. Next, 100 μL of 28% ammonia solution was added, and then 1.5 mL of 30% hydrogen peroxide was introduced into the mixture at a rate of one drop every 10 sec. The reaction mixture was stirred in an ice bath for 2 h before being quenched to a pH of 11.5 using 0.5 M NaOH. A change in the color of the suspension from slightly cloudy to completely white indicated the formation of CaO_2 NPs. The suspension was centrifuged at 15 000 rpm 4°C for 5 min, and the resulting white precipitate was identified as CaO_2 NPs. The particles were washed twice with 0.5 M NaOH, followed by two washes with distilled water and two washes with absolute ethanol. To ensure the collected NPs were homogeneously dispersed, the suspended CaO_2 NPs in ethanol were sonicated using a sonication machine (Bioruptor BR-II) under 30 sec "on;" 30 sec "off," 20 KHz for 1 h in a 50 mL tube kept at 4°C. Afterward, the white color suspension of synthesized nanoparticles was obtained. Evaluation of obtained yield was further studies, 1 mL of the suspended CaO_2 NPs in ethanol was centrifuged at 5000 rpm for 3 min. The supernatant was removed, and the remaining precipitate was dried under vacuum overnight. The weight of the nanoparticles in 1 mL of solution was averaged from three different test tubes. The synthesized nanoparticles were confirmed using X-ray diffraction analysis (XRD; Malvern Panalytical, Malvern, U.K.), and the surface morphology was visually investigated after treatment with osmium for 30 sec using a scanning electron microscope (SEM; JSM-7601F, JEOL Ltd., Tokyo, Japan) at an accelerating voltage of 10 kV.

4.3 | Synthesis of γ-PGA-Aln and γ-PGA-Aln-Phe

The synthesis of γ-PGA-Aln and γ-PGA-Aln-Phe was synthesized similar to previous reported [32]. For γ-PGA-Aln, 1.0 g of γ-PGA (7.7 mmol) was dissolved in 100 mL of 0.20 M $NaHCO_3$ (aq.) following with the addition of 2.1 g of DMTMM (7.7 mmol) and let it react for 10 min before adding 1.9 g of Aln (7.7 mmol). The pH of the reaction was adjusted to pH 8.2 using 5 M NaOH (aq.) and stirred for 24 h at room temperature. The reaction was collected and purified via dialysis against absolute ethanol (MWCO 12 000 ~ 14 000 Da) for overnight and water for 3 days. White product was obtained after lyophilization for 3 days. The ratio of the synthesis was as summarized in Table S1. Similarly, the synthesis of γ-PGA-Aln-Phe was performed using γ-PGA-Aln as a starting material. The reaction was carried out starting from the ratio of 1.0:1.0:1.0 molar ratio between γ-PGA-Aln, Phe, and DMTMM based on the remaining carboxyl group on the γ-PGA-Aln. The reaction was begun with dissolving 0.30 g of γ-PGA-Aln10 (2.1 mmol) in 30 mL of 0.20 M $NaHCO_3$ and mixed with 0.59 g of DMTMM (2.1 mmol) for 10 min. 0.49 g (2.1 mmol) of Phe was then added and allow the reaction to react for 24 h at room temperature. The solution was then purified under precipitated in EtOH solution and centrifuge at 10 000 rpm for 10 min thrice before redissolved in DMSO/water (50/50) and dialysis against DMSO/water (50/50) for 2 days and water for 3 days, respectively (MWCO 12 000 ~ 14 000 Da). White product of γ-PGA-Aln-Phe was obtained after lyophilization. The products from both synthesized polymers were then further characterized and calculate its grafting degree using ^{1}H-NMR (400 MHz, D_2O, ppm) 25°C under 64 scans. Various grafting degrees of the Phe group were synthesized based on the reaction ratios provided in Table S4.

4.4 | Fabrication of Oxygen-Releasing Hydrogel

The hydrogel was formed by mixing a polymer solution with a dispersed CaO_2 nanoparticle (NPs) solution using the vortex method. To prepare the hydrogel, a stock solution of 10% w/w γ-PGA-Aln polymer in 500 mM phosphate buffer (PB) (pH 7.0) was prepared. A sample bottle (Product code 84–0721, model No. 02) with a diameter of 12 mm was used as the container for the hydrogel formation. For a final hydrogel volume of 400 µL (volume ratio of γ-PGA-Aln: CaO_2 NPs = 8:2), 320 µL of the polymer stock solution was added to the sample bottle. Then, 80 µL of suspended CaO_2 NPs absolute EtOH containing different concentration of 0.5, 1, 2, 3, and 4 wt% was added in to the mixing bottle, respectively. Due to the optimization, volume ratio between polymer solution and NPs content will keep constant at 8:2 throughout the study. The mixture was vortexed using a Taitec Presentmixer 2013 (No. 3050319) at a fixed vibration speed of 2800 r/min for 10 sec (supplementary video 1). Next, effect of polymer concentration, polymer solution in different PB concentration, different Aln grafting degree, and varying CaO_2 NPs concentrations toward fabrication of oxygen-releasing hydrogel was evaluated using the same preparation method. The confirmation of the gelation of each condition was performed using vial-tilting method.

4.5 | Compression Analysis

A cylindrical hydrogel prepared in the previous step, with a diameter of 10 mm and a height of 4 mm, was subjected to mechanical testing using a universal testing machine (Autograph AGS-X, Shimadzu Corp., Kyoto, Japan) equipped with a 20 N load cell. Each sample was placed on the lower plate and compressed by the upper plate at a strain rate of 5 mm min^{-1}. The elastic modulus of the samples was calculated as the slope of the stress-strain curve within the 5% to 10% strain range. In addition, to understand the effect of oxygen released from the oxygen-releasing material on the hydrogel, the mechanical properties of the gel were analyzed at different time point. Specifically, after the hydrogel was formed using the vortex method, it was left at room temperature for intervals of 30, 60, 120, and up to 1440 min before undergoing compression testing using the described set-up.

4.6 | Scanning Electron Microscope Imaging and X-Ray Diffraction Analysis

The morphological characterization of hydrogel was observed under a SEM (Phenom ProX G6 Desktop SEM, Thermo Fisher scientific). Subject hydrogel was frozen in liquid N_2 for 15 min before lyophilized for 24 h or until completely dry (FDU-2200, EYELA, Tokyo, Japan). Dried hydrogel was vertically sections and osmium (HPC-30 Plasma Coater, Vacuum Device, Ibaraki, Japan) on cross-sectioned surface for 30 sec and observed under high vacuum conditions at an accelerating voltage of 10 kV for Desktop SEM and their composition were analyzed with an X-ray energy dispersive spectroscope (EDS) (Phenom ProX G6 Desktop SEM, Thermo Fisher scientific). Crystalline structure of dried hydrogel was analyzed using X-ray diffraction (XRD) analysis. The obtained oxygen-releasing hydrogel was first dried under lyophilization for 2 days and crushed into small pieces before further XRD measurement (AERIS, Malvern Panalytical, Malvern, U.K.).

4.7 | Fabrication of γ-PGA-Aln Hydrogel With Alternative Polysaccharides, Divalent Cations and Peroxide Sources

To investigate the role of polymer-nanoparticle interactions, γ-PGA-Aln was substituted with alternative polysaccharide polymers known for their divalent cation crosslinking capabilities, including sodium alginate (CAS 9005-38-3, Sigma-Aldrich) and κ-carrageenan (CAS 1114-20-8, Sigma-Aldrich). Specifically, a 5% (w/v) solution of each polysaccharide was prepared in 500 mM phosphate buffer (PB, pH 7.0). 320 µL of the polymer solution was subsequently mixed with 80 µL of a 1 wt% suspension of CaO_2 NPs. Each polymer solution was further vortexed for 10 sec. The obtained gel was further evaluated using the vial-tilting method. To understand the selectivity of the CaO_2 NP interaction, γ-PGA-Aln was further mixed with different cations and peroxide compounds. For divalent cation testing, 1 wt% of $CaCl_2$, $BaCl_2$, $MgCl_2$, and $MnCl_2$ were slowly added to a 10% w/w of γ-PGA-Aln solution prepared using deionized (DI) water, vortexed for 1 min and checked for gelation through tube-tilting

method. Similarly, γ-PGA-Aln was mixed with different peroxide compounds, including commercially available micron-size CaO_2 particles, BaO_2 and MgO_2 to observed gelation ability. Any sample that successfully formed a hydrogel was subsequently analyzed for its compressive strength using the same set-up described in the compression analysis section.

4.8 | Fabrication γ-PGA-Aln-Phe-Based Oxygen-Releasing Hydrogel and Stability Assessment

The conjugation of a hydrophobic segment onto the polymer chain was expected to enhance the stability of the fabricated material in aqueous solution over time. Therefore, γ-PGA-Aln10-Phe was further evaluated for its gelation ability and stability. γ-PGA-Aln10-Phe-based oxygen-releasing hydrogel was fabricated following the procedure as described above with slight modifications. Specifically, 320 μL of 10% w/w γ-PGA-Aln10-Phe in 1 M PB (pH 7.0) was prepared and mixed with 80 μL of 1 wt% CaO_2 NPs for 10 sec. The stability of the oxygen-releasing hydrogel, with and without the hydrophobic segment, was assessed by monitoring changes in diameter during incubation in serum-free Dulbecco's modified Eagle's medium (DMEM) (08458-45, Nacalai Tesque, Kyoto, Japan) at 37°C. Cylindrical samples (10 mm diameter, 4 mm height) were initially measured at 0 min, and changes in diameter were recorded at various time points to evaluate structural stability over time.

4.9 | Conjugation of Fluorescein Isothiocyanate to Catalase

To keep track of catalase in the experiments, the conjugation of FITC [71] with catalase was first prepared. Briefly, 1 mg/mL of catalase was dissolved in 20 mL phosphate buffer (pH 8). Next, 1.5 mL of 1 mg/mL FITC (3326-32-7, Sigma-Aldrich) in dimethyl sulfoxide (DMSO) was mixed with 20 mL catalase solution for 1 h at room temperature. The FITC-labeled catalase was purified and separated from unreacted FITC through dialysis against 3 L of 500 mM PB (pH 7.4) (MWCO 3500 Da) for 2 days. Dialysis media was changed once a day. The dialyzed solution was then lyophilized to obtain a yellowish product.

4.10 | Positioning of FITC-Label Catalase and Morphological Analysis

To achieve clearer imaging of fluorescence signals within constructed hydrogel, the hydrogel either coated for 1 h or mixed for 10 sec with FITC-labeled catalase was further evaluated to determine the positioning of catalase through fluorescence imaging. After confirmation of stability of γ-PGA-Aln10-Phe-based oxygen-releasing hydrogel. The formulation of 10% w/w γ-PGA-Aln10-Phe55 in 1 M PB with 1 wt% CaO_2 NPs was selected as an optimal for remainder study. For mixing method, freshly prepared 200 μL hydrogel consisting of 160 μL of 10% w/w γ-PGA-Aln10-Phe55 (1 M PB) and 40 μL of 1 wt% CaO_2 NPs, together with 10 U FITC-labeled catalase was fabricated. Constructed hydrogel was then horizontally sectioned in half and placed on a 24-well plate. Fluorescence imaging of each condition was taken using CQ1 (confocal quantitative image cytometer). On the other hand, for the coating method, confirmation of coating efficiency under different catalase concentration was first evaluated. Different catalase concentrations ranging from 0, 10, 50, 100, and 200 U/mL in phenol red and serum free DMEM (1% antibiotics) was prepared for the coating. In addition, optimization of the coating process under different incubation times was also evaluated. After optimization, the oxygen-releasing hydrogel was immersed in 200 U/mL catalase at 4°C for 1 h and used for further evaluation. Phase contrast image and fluorescence intensity across the sectioned gel was analyzed and averaged using ImageJ software. Furthermore, the same condition was replicated, and the sample were lyophilized for 24 h before being horizontally sectioned. The sectioned gel was treated with osmium for 30 sec and further observed for morphological structure using Desktop SEM (Phenom ProX G6 Desktop SEM, Thermo Fisher scientific) under accelerating voltage of 10 kV.

4.11 | Effect of Coating and Mixing Catalase to Mechanical Property

A total of 200 μL of constructed hydrogel that prepared in round bottom safe-lock Eppendorf tube, given a hydrogel with a diameter of 7 mm and a height of 3 mm was fabricated. The mechanical properties of the hydrogel were then evaluated after mixing and coating with 10 U catalase. Next, catalase-coated (immerse at 4°C for 1 h) and catalase-mixed sample (10 sec mixing) were then incubated in phenol red- and serum-free DMEM (1% antibiotics). Mechanical testing was performed either immediately after catalase incorporation (defined as 0 min; immediately after mixing or after 1 h coating) or after 24 h incubation at 37°C.

4.12 | Evaluation of H_2O_2 Release

To explore the catalase activity on inhibiting hydrogen peroxide (H_2O_2) release, the remaining of H_2O_2 concentration in phenol red- and serum-free DMEM (08489-45, Nacalai Tesque) containing hydrogel was evaluated using Oxiselect Hydrogen Peroxide/ Peroxidase Assay Kit (Fluorometric) (STA-344, Cell Biolabs Inc., San Diego). 100 μL of oxygen-releasing hydrogel was further coating and mixing with 10 U catalase before rinsing with PBS and incubated in 1 mL of phenol red- and serum-free DMEM (1% antibiotics) in a 24-well plate at 37°C. Samples were incubated in different time points, including 1 h, 1, 2, 3, 4, and 5 days. According to the detection limit specified in the assay kit protocol, each sample was diluted 1000 times using assay buffer. A 50 μL aliquot of the diluted sample from each time point was mixed with 50 μL of the assay kit's working solution in a black 96-well plate. The samples were left at room temperature for 30 min before measuring fluorescence intensity using a microplate reader (SYNERGY/HTX multimode reader, BioTek Instruments, Winooski) with excitation and emission wavelengths of $\lambda_{ex} = 540$ nm and $\lambda_{ex} = 590$ nm, respectively. Result from the measurement was compared and calculate according to standard curve of known concentrations of hydrogen peroxide ($0 \sim 1.56$ μM).

4.13 | Oxygen Release Profile Under Hypoxic Conditions

100 μL oxygen-releasing hydrogel as mentioned in previous section was prepared. 10 and 200 U/mL catalase in 1 mL phenol red- and serum-free DMEM (1% antibiotics) was used as medium for coating method. While 10 U of catalase was applied for the mixing condition, as the concentration of 200 U caused instability and collapse of the hydrogel after 1 h of incubation. The dissolved oxygen levels in DMEM including hydrogel were measured under a hypoxic condition using as SDR SensorDish Reader (SDRSensorDishReader, PreSens, Regenburge, Germany), following the set-up and analysis method detailed in a previous report [31]. Freshly prepared 100 μL samples of hydrogels coated with 10 U/mL and 200 U/mL catalase, as well as hydrogels mixed with 10 U catalase were place in a 24-well sensor dish (OxoDishOD24, PreSens, Regenburge, Germany). Each sample was then immersed in 1 mL of phenol red- and serum-free DMEM (1% antibiotics). Medium without hydrogel immersion was used as a control. To create a hypoxic environment, the SensorDish Reader and the 24-well sensor dish were placed in a hypoxia cell culture airtight bag (6-8669-03, As One, Osaka, Japan) containing three Anaero Pack O_2 absorbers (Mitsubishi Gas Chemical Company Inc., Tokyo Japan) and sealed with parafilm. The dissolved oxygen levels were monitored at 37°C every 15 min for 3 days. The obtained data were averaged from triplicate independent measurement.

4.14 | 2D-Cytotoxicity Toward NHDF Cells

Cytocompatibility of the oxygen-releasing hydrogel was assessed using the WST-8 (CCK-8) assay. Normal human dermal fibroblasts (NHDFs) were seeded into 24-well plates at a density of 1.25×10^4 cells/cm^2 and incubated overnight in 500 μL supplemented DMEM (10% FBS and 1% antibiotics) at 37°C in 5% CO_2 to allow cell adhesion. 100 μL of oxygen-releasing hydrogels with and without catalase coating were prepared. For catalase coating, hydrogels were treated with 200 U/mL catalase, rinsed three times with PBS, and placed into cell culture inserts (Grenier bio-one ThinCert, pore size 0.4 μm). Inserts containing hydrogels were transferred to wells containing adhered NHDFs (Figure S5a) and incubated in the same volume of 500 μL supplemented DMEM (10% FBS and 1% antibiotics) inside and outside the insert. Cultures were maintained under hypoxic conditions (O_2< 0.1%) using a gas barrier box (As One, GB-2.0 L, Osaka, Japan) containing two AnaeroPack O_2 absorbers at 37°C, 5% CO_2. WST reagent was prepared by mixing transparent DMEM with Cell Count Reagent SF (08458-16, Nacalai Tesque, Kyoto, Japan). After 3 days, cells were washed with PBS, treated with 200 μL of WST reagent, and incubated for 1 h under standard culture conditions. Subsequently, 100 μL of the supernatant was transferred to a 96-well plate, and absorbance was measured at 450 nm using a microplate reader (Model 680, Bio-Rad Laboratories, Inc, Japan). Cell numbers were calculated based on a standard curve generated from the relationship between absorbance values and known cell counts. Phase-contrast images of each sample were obtained after 3 days of culture using an EVOS XL Core Imaging System (Thermo Fisher Scientific, MA, USA).

4.15 | Intracellular Reactive Oxygen Species (ROS) Assay

Intracellular ROS levels were measured using the ROS Detection Cell-Based Assay Kit (DCFDA) (Cat. 601520, Cayman Chemical). Cell seeding density and hydrogel conditions were prepared as described in the cytotoxicity assay. NHDFs were seeded at 1.25×10^4 cells/cm^2 into 24-well plates and cultured overnight in 500 μL supplemented DMEM (10% FBS, 1% antibiotics) at 37°C in 5% CO_2 incubator to allow cell attachment. On the following day, 100 μL of oxygen-releasing hydrogel, with or without 200 U/mL catalase coating, was fabricated and placed into a cell culture insert (Grenier bio-one ThinCert, pore size 0.4 μm) positioned over the pre-attached NHDFs. Cultures were maintained under normoxic conditions (O_2> 21%, 37°C, 5% CO_2) for 24 h. Cells that did not exposed to hydrogels was use as controls. After incubation, cells were washed with cold PBS and lysed with 250 μL/well of 1% Triton X-100 in PBS, followed by a 10 min incubation on ice. Samples were collected by scraping, sonicated for 10 min, and centrifuged at 12 000 rpm for 5 min. 50 μL of the supernatant was transferred into a black 96-well plate, while 20 μL was collected for DNA quantification. For ROS detection, 100 μL of 10 μM DCFDA in PBS was added to each well of the black plate. The plate was incubated for 30 min at 37°C, 5% CO_2, protected from light. Fluorescence intensity was measured at an excitation wavelength of 485 nm and an emission wavelength of 538 nm using a microplate reader (Model 680, Bio-Rad Laboratories, Japan). Total DNA content was determined according to the Qubit manufacturer's instructions (Qubit 1X dsDNA HS Assay Kit, Cat. Q33230, Thermo Fisher Scientific). Briefly, 20 μL of supernatant was mixed with 180 μL of Qubit working solution, incubated at room temperature for 3 min, and measured with a Qubit 3.0 Fluorometer (Thermo Fisher Scientific, Waltham, MA). ROS levels were normalized to DNA content and expressed as a percentage relative to the control. Results were reported as mean ± SD from triplicate independent experiments.

4.16 | Fabrication of Millimeter-Size Scaffold and Culture Under Hypoxic Conditions of NHDF Cells

The construction of fibrin gel for 3D tissue was adapted from a previous study by M. Piantino et al. [72]. Briefly, 100 μL of 24 mg/mL fibrinogen (Ref. F8630-5G, Sigma-Aldrich, St. Louis, MO, USA) was dispersed in 100 μL of non-supplemented DMEM in an Eppendorf tube. In a separate tube, 1.5×10^6 NHDF cells were dissociated in 100 μL of 12 U/mL thrombin (T4648-10kU, Sigma-Aldrich, St. Louis, MO, USA) with an additional of 100 μL of supplemented DMEM (10% FBS and 1% antibiotics). The final concentrations of fibrinogen and thrombin in a total 400 μL fibrin gel were 6 mg/mL and 3 U/mL, respectively. Prior to fibrin gel formation, total volume of 100 μL oxygen-releasing hydrogel was prepared. The hydrogel was cut into four equal pieces, washed three times with serum- and phenol red-free DMEM (1% antibiotics), and incubated in 1 mL of serum- and phenol red-free DMEM containing 200 U/mL catalase for 1 h at 4°C. In a separate Eppendorf tube, equal volumes of fibrinogen solutions were mixed to a final volume of 400 μL and immediately transferred into a 48-well plate. Subsequently, a quarter segment of the catalase-coated oxygen-releasing hydrogel was placed into fibrin solution. As a control, fibrin gels with 1.5×10^6 NHDF cells alone

and those embedded with non-catalase-coated oxygen-releasing hydrogels were prepared. All samples were incubated at 37°C, 5% CO_2 for an additional 1 h to ensure complete gelation. Then, each sample was individually place into 6-well plate containing 5 mL supplemented DMEM (10% FBS, 1% antibiotics) and 5 μg/mL aprotinin (CAS 9087-70-1, 50 000 KIU, Fujifilm Wako) to prevent fibrin degradation. The sample was further culture under hypoxic conditions using a gas barrier box (GB-2.0 L, As One, Osaka, Japan) containing two AnaeroPack O_2 absorbers at 37°C, 5% CO_2. Assessment of total DNA number was measured at day 5 and day 10 of culture.

4.17 | Assessment of Total DNA Number

After 5 and 10 days of culture of millimeter-size scale scaffolds under hypoxic condition, scaffolds were rinsed with PBS before performing cell viability by quantifying total DNA content. The scaffold was first lysed by addition 900 μL of ATL lysis buffer (Qiagen) and 100 μL of Proteinase K, followed by incubation at 56°C for 2 h until the fibrin gel was completely degraded. 10 μL of sample was then mixed with 190 μL Qubit working solution and incubate for 3 min at room temperature before quantify using Qubit 3.0 Fluorometer (Thermo Fisher Scientific, Waltham, MA) with the Qubit 1× dsDNA HS Assay Kit (catalog no. Q32854, Thermo Fisher Scientific). A 2D culture of initial cell seeding (1.5×10^6 cells of NHDF) in 6-well plate was prepared in parallel to determine relative cell viability and the cell pallets was collected and lysed after 8 h of culture. Total DNA number in 3D scaffold was expressed relative to the DNA amount of the initial seeding population. Results are presented as the mean ± SD from three independent experiments.

4.18 | Live/Dead Analysis and Immunofluorescence Staining of Millimeter-Size Scaffold

The distribution of viable/dead cell within construct scaffold was assessed after 5 days of culture. Samples were rinsed with PBS and incubated in 1000 μL of PBS containing 1 μL of Calcein AM (Invitrogen), 4 μL of ethidium homodimer (EtHD-1, Sigma), and 1 μL of Hoechst 33342 (Invitrogen) at room temperature for 1 h. After incubation, samples were washed twice with PBS and observed using a confocal laser scanning microscope (CLSM), FluoView FV3000 (Olympus, Tokyo, Japan). Obtained image was used for further quantitative analysis for evaluation of viable cells within each condition of scaffold using Ilastik (v1.4.1) and CellProfiler (v4.2.8). Total viable cells were calculated and expressed relative to nuclei number. For each sample, three fields of view specifically inside the matrix and near to hydrogel region was captured, with a consistent z-stack thickness of 150 μm. Results are presented as mean ± SD from four independent experiments. In addition, cell morphology was demonstrated using immunofluorescence staining. After 5 days of culture, scaffolds were fixed with 4% paraformaldehyde (PFA) for 30 min at 4°C. After being rinsed twice with PBS, sample were permeabilized in with 0.2% Triton X-100 in PBS for 15 min at room temperature under gently agitation (50 rpm). Samples then washed three times with PBS before being incubated overnight at 4°C with PBS containing 1% bovine serum albumin (BSA; Sigma-Aldrich), Alexa Fluor 488 Phalloidin (1:800 dilution; Invitrogen) for F-actin filaments and 4',6-diamidino-2-phenylindole (DAPI) (1:1000 dilution; Gibco) for nuclei staining. The image was further observed by CLSM.

4.19 | Fabrication of Centimeter-Sized Scaffold

Construction of large-scale scaffold, specifically, centimeter-size scale scaffold was further fabricate using sandwich approach. Prior formation of fibrin gel, 6 mg/mL fibrinogen solution in serum free DMEM (1% antibiotics) and 3 U/mL of thrombin containing 15×10^6 NHDFs/ mL in supplemented DMEM (10% FBS, 1% antibiotics) was individually prepared. A cylindrical mold (5 mm diameter and 2 mm height) was autoclaved prior use. Unlike millimeter-size scaffold, full size of 100 μL catalase-coated oxygen-releasing hydrogel (5 mm diameter and 1.25 mm height) was fabricated. Scaffold assembly was performed by sequentially layering fibrinogen and thrombin solutions into the mold. First, 500 μL of fibrinogen solution and 500 μL of thrombin solution were mixed in the mold, followed by placement of the full-size hydrogel in the center, and allowed to gel for 5 min at room temperature. Next, an additional 500 μL each of fibrinogen and thrombin solutions were added to form the second layer. The entire construct was polymerized for 1 h at 37°C in a humidified incubator (5% CO_2) before being transferred to a 6-well plate containing 10 mL of supplemented DMEM (10% FBS, 1% antibiotics) and 5 μg/mL aprotinin. Scaffolds without oxygen-releasing hydrogels and with non-catalase-coated hydrogels were prepared as controls. Cultures were maintained for 5 days in a gas-barrier box with two AnaeroPack O_2 absorbers to establish hypoxic conditions. The culture medium was refreshed on day 3 using DMEM pre-equilibrated overnight under hypoxia conditions to minimize reoxygenation effects. After 5 days of culture, scaffolds were analyzed for cell distribution using light-sheet fluorescence microscopy (LSFM) and determine viable cells via Live/Dead staining. To acquire complete Live/Dead staining within thick constructs rather than only at the outer regions of the scaffold, the scaffolds were vertically sectioned prior to staining, following the procedure described earlier. Fluorescence imaging was performed above the cutting plane to minimize potential artifacts or false-positive signals arising from cell damage at the cut surface. This enabled accurate evaluation of cell distribution and viability within the inner regions of the construct. Total viable cells were calculated and expressed relative to nuclei number. Results are presented as the mean ± SD from 15 independent areas.

4.20 | Hypoxia Analysis by LOX-1 Hypoxia Probe

Hypoxia within the centimeter-scale scaffold was evaluated using the LOX-1 hypoxia probe (Medical & Biological Laboratories, Japan). Centimeter-sized scaffolds were prepared as described previously, with scaffolds in the absence of the oxygen-releasing hydrogel used as the control group. The samples were cultured under hypoxic conditions, and LOX-1 staining was performed according to the manufacturer's protocol. Briefly, the culture medium was first pre-equilibrated under hypoxic conditions overnight. Fresh 2 μM LOX-1 was then added to the pre-hypoxia-calibrated medium, and the samples were cultured for an

additional 24 h prior to detection. On the day of imaging, the scaffolds were vertically sectioned into halves to enable observation of the internal region. Full-size LOX-1 fluorescence mapping across the scaffold was observed using an FV3000 confocal microscope. The fluorescence intensity settings and acquisition thickness (50 μm) were kept constants for all samples. LOX-1 fluorescence intensity throughout the scaffold was quantified using the "Raw Intensity Heatmap Grid" macro in ImageJ with a window size of 200 × 200, and the obtained data were further analyzed using Prism software. In addition, fluorescence intensity gradient profiles within the hydrogel were quantified using ImageJ. Analysis was performed along the dotted line indicated in the fluorescence images, extending from the oxygen-releasing hydrogel region toward the peripheral region of the scaffold. Quantification of LOX-1-positive cells was performed using IMARIS. 10 random images from the inner region of the scaffold were selected and analyzed for LOX-1-positive cells, which were normalized to the total number of nuclei. Data are presented as mean ± SD from three biological replicates, except for the control group, which is presented from one fabricated biological sample.

4.21 | Light-Sheet Fluorescence Microscopy

Full image analysis of centimeter-scale scaffolds was performed after 5 days of culture under hypoxic conditions. Whole-scaffold imaging was conducted using a ZEISS Lightsheet 7 system. Scaffolds from each condition were fixed and permeabilized following the same procedure described for immunofluorescent staining, with extended incubation times to accommodate the larger scaffold size. Scaffolds were fixed in 4% paraformaldehyde for 1 h at 4°C, rinsed three times with PBS, and incubated overnight at room temperature with gentle agitation in PBS containing 1% (w/v) BSA, Alexa Fluor 488 Phalloidin (1:800 dilution), and DAPI (1:1000 dilution). After three additional PBS washes, scaffolds were incubated in RapiClear 1.47 (SUNjin Lab) at 37°C overnight for optical clearing. The cleared scaffolds were then positioned within the ZEISS-provided holder, embedded in RapiClear CS mounting gel (SUNjin Lab), and allowed to solidify at 4°C for 30 min. Fluorescence images were subsequently acquired using LSFM.

4.22 | Culture of Human Neural Stem Cells Maintenance

Human neural stem cells (hNSCs) derived from the NIH-approved H9 (WA09) human embryonic stem cell line was obtained from Life Technologies as a commercially available product (N7800-200). Cells were handled and culture accordance to manufactured protocol and as mentioned in previous protocol [73] Briefly, prior cell seeding, polystyrene plates (Corning) were first coated with 20 μg/mL poly-L-ornithine (Sigma-Aldrich) following by 10 μg/mL of Laminin (L2020, Sigma-Aldrich). hNSCs were cultured in expansion medium, namely StemPro NSC SFM medium supplemented with basic fibroblast growth factor (bFGF, 20 ng mL^{-1}), epidermal growth factor (EGF, 20 ng mL^{-1}), (all Gibco), and 1% v/v penicillin-streptomycin (pen-strep). Cells were initially seeded at a density of 1×10^5 cells/cm^2 and subsequently passaged when they reached approximately 90% confluence.

4.23 | Indirect Cytotoxicity Tests Using hNSCs

To evaluate the cytocompatibility of catalase-coated oxygen-releasing hydrogel toward hNSC, indirect cytotoxicity tests were performed using resazurin (Sigma-Aldrich) and LDH release analysis (Invitrogen). hNSCs were seeded in 24-well plates at a density of 3×10^4 cells/cm^2 and cultured overnight to allow cell adhesion. Full-sized catalase-coated oxygen-releasing hydrogels were prepared as described above and washed prior use. The hydrogels were placed into transwell inserts (Grenier bio-one ThinCert, pore size 0.4 μm) (one hydrogel/insert), followed by the addition of 500 μL of supplemented culture medium to the inner part of the inserts. The inserts were then transferred to the hNSC-seeded wells and incubated under normoxia (O_2 > 21%) and severe hypoxic (O_2< 0.1%) conditions for 24 h. After 24 h of culture, the inserts were removed, and 50 μL of cell supernatant were transferred to the wells of a 96-well plate for subsequent LDH release assay. The remaining culture medium in each well was removed and replaced with culture medium containing 20% (v/v) resazurin sodium salt (Sigma-Aldrich) in PBS. The plates were incubated for an additional 2-h period under the same oxygen conditions. Afterward, 100 μL of the supernatant were transferred into the wells of black 96-well plates (Greiner Bio-one), and fluorescence intensity was measured using microplate plate reader (BioTek Synergy Mx) with an excitation wavelength of 530 nm and an emission wavelength of 590 nm. The relative fluorescence unit (RFU) was expressed as percentage of the correspondent control, namely cells cultured in the absence of the oxygen-releasing hydrogel (Figure S11a)

In addition, LDH assay was quantified using CyQUANT LDH cytotoxicity assay kit according to the manufacturer's instructions. The cell supernatants collected previously were mixed with the LDH reaction reagent and incubated for 30 min at room temperature, protected from light. After incubation, the optical density at 490 nm and 690 nm was measured using a microplate reader. Cytotoxicity was quantified according to the manufacturer's protocol. Cells cultured without the oxygen-releasing hydrogel were lysed with the kit's Lysis Buffer to establish the maximal LDH activity:

$$\%\text{cytotoxicity} \left(\frac{\text{Compound treated LDH activity} - \text{Spontaneous LDH activity}}{\text{Maximum LDH activity} - \text{Spontaneous LDH activity}}\right) \times 100$$

4.24 | Oxygen Content Within Fibrin Gel

To validate oxygen release under the fibrin gel configuration, the dissolved oxygen content was re-evaluated using an embedded hydrogel setup. To maintain the oxygen-releasing hydrogel at the center of the fibrin gel construct, a polydimethylsiloxane (PDMS) mold was used to create a cavity within the central region of the gel. Briefly, a first layer of acellular fibrin gel was deposited as illustrated in Figure S12a(i) and incubated at 37°C for 1 h. After complete gelation, the PDMS mold was removed. One-quarter of the oxygen-releasing hydrogel coated with 200 U/mL catalase at 4°C for 1 h was subsequently positioned within the central cavity of the first fibrin gel layer. A second layer of fibrin polymerizing solution was then added to fully embed

the material (Figure S12a(ii)), followed by incubation at 37°C for an additional 1 h to allow complete gelation. Catalase-coated oxygen-releasing hydrogels merely immersed in 400 µL of the buffer used for fibrin gel preparation (1× TBS, pH 7.4) were also assessed. Dissolved oxygen measurements for both fibrin-embedded and non-embedded samples were performed under the same experimental setup described above. The reported data represent the net increase in dissolved oxygen after subtraction of the deoxygenation profile obtained from the medium-only control.

4.25 | Culture of hNSCs Within Fibrin Gel in the Presence of Catalase-Coated Oxygen-Releasing Hydrogel

hNSCs were dissociated into single cells using StemPro accutase cell dissociation reagent (Gibco) and resuspended in the fibrinogen solution before the addition of equal volume of thrombin solution containing $CaCl_2$. A PDMS mold (3 mm diameter × 7 mm height) was placed at the center of each well in a 48-well plate, and 200 µL of the fibrin polymerizing solution containing dissociated cells (1×10^6 cells/mL) were added to the each well for the formation of the hNSC-laden fibrin gel layer. This step generated a central cavity for subsequent addition of the oxygen-releasing hydrogel (Figure S12a). The fibrin gels were incubated in 37°C in a 5% CO_2 humidified incubator for 1 h to allow fibrin gel cross-linking by factor XIIIa. After gelation, the PDMS mold was removed and 400 µL of supplemented StemPro NSC SFM containing 5 µg/mL aprotinin were added to each well. Constructs were cultured for 2 days under humidified conditions at 37°C and 5% CO_2 to allow initial cell proliferation. On day 2, the medium was aspirated, and a quarter section of the catalase-coated oxygen-releasing hydrogel prepared as described for the millimeter-scale scaffold, was transferred to the central cavity. An additional 200 µL of acellular fibrin polymerizing solution were then added to each well, to ensure the central positioning of the embedded hydrogel. The crosslinking of the second fibrin layer was achieved as described above. Once fully set, the entire construct was transferred to the wells of a 6-well plated previously filled with 5 mL of neuronal differentiation medium, which consisted of a (1:1) mix of StemPro NSC SFM media without growth factors and Neurobasal/B27 medium (Neurobasal medium supplemented with 2% v/v B27 and 1% v/v L-glutamine, all Gibco), containing 5 µg/mL of aprotinin. On day 8 of culture, half of the culture medium was replaced by StemPro NSC SFM: Neurobasal/B27 (1:3 mix), supplemented with 10 ng/mL of recombinant human BDNF (Peprotech), 500 µM of dibutyryl cAMP (Sigma), and 5 µg/mL of aprotinin. Cell-laden hydrogels were cultured for periods up to 12 days, half of medium being renewed every other day (Figure S12b). The cultures were kept in a controlled severely hypoxic environment using a humidified PhO_2X Box cell culture chamber (Baker Ruskinn) with a controlled atmosphere of 0.1% O_2 and 5% CO_2, which was placed in the 37°C incubator.

4.26 | Cell Metabolic Activity and Live/Dead Assay in hNSC-Laden Fibrin Gels

The metabolic activity and the distribution of viable/dead cells within fibrin gel were assessed using resazurin and a Live/Dead assay, respectively. The cell metabolic activity of embedded hNSCs, in the absence or presence of catalase-coated oxygen-releasing hydrogels, was evaluated on day 1, 3, 5, and 12 of differentiation. At each time point, the cell-constructs were transferred to fresh neuronal differentiation medium containing 20% (v/v) resazurin sodium salt and incubated for 2.5 h at 37°C, 5% CO_2, under the same severe hypoxic conditions used during culture. Subsequently, 100 µL of the supernatants were collected for spectrophotometric analysis, and the samples transferred back to the initial wells to continue the culture until day 12. Results are presented as mean ± SD from three independent experiments, each performed with four technical replicates.

The Live/Dead assay was performed on day 1 and day 12 of cell culture. Samples were rinsed with PBS and incubated for 30 min at 37°C, 5% CO_2, in pre-warmed PBS containing Calcein-AM (4 µg/mL, Thermo Fisher Sci.), ethidium homodimer (2 µg/mL, Sigma), and 2.5 µg/mL Hoechst 33342 (Thermo Fisher Sci.). Fluorescent image stacks covering a thickness of 150 µm were acquired using Leica TCS SP5 confocal Microscope (Leica Microsystems). At least 6 fields of view were acquired at different positions throughout the gel. The percentage of viable cells was calculated in relation to the total nuclei per image. Results are presented as the mean ± SD from three independent experiments. For each experiment, six images were analyzed and the average percentage of viable cells was determined.

4.27 | Isolation of hNSCs From Fibrin Gel

The constructs were washed with PBS and sequentially incubated with 3 mg/mL nattokinase solution (NSK-SD) for 1 h at 37°C, followed by incubation in 1× trypsin-EDTA (30 min at 37°C; Gibco), both steps under mild agitation (70 rpm). After trypsin inactivation with serum-containing media cells were mechanically dissociated by pipetting and pelleted by centrifugation. After being resuspended in 1× PBS, cells were counted using the trypan blue exclusion dye, centrifuged, and the cell pallets stored at −80°C.

4.28 | Total DNA Quantification in hNSC-Laden Fibrin Gels

Cell pellets isolated from fibrin gels were lysed with 250 µL of 1% Triton X-100 in PBS and incubated on ice for 10 min, followed by sonication for 10 min and centrifugation at 12 000 rpm for 5 min. Subsequently, 10 µL of the supernatant was mixed with 190 µL of Qubit working solution, and total DNA content was quantified using the same Qubit 2.0 Fluorometer protocol described above. DNA content was expressed as total DNA (ng) per fibrin matrix. Results are presented as mean ± SD from three independent experiments.

4.29 | Immunostaining of hNSC-Laden-Fibrin Gels

At the end of the culture time, the cell-laden fibrin gels were processed *en-bloc* for immunofluorescence labelling of Nestin,

βIII-Tubulin, and MAP2. Briefly, samples were washed trice with PBS and fixed with 4% (w/v) paraformaldehyde (PFA, Sigma-Aldrich) for 20 min, at room temperature. After rinsing with PBS, they were permeabilized in PBS containing 0.2% (v/v) Triton X-100 (PBS-T, Sigma-Aldrich) for 45 min at room temperature under gentle stirring on an orbital shaker. Following permeabilization, the cell-constructs were washed trice with PBS and blocked for 60 min at room temperature in PBS buffer containing 5% (w/v) Normal Donkey Serum (NDS), 3% (w/v) BSA, and 0.05% Tween-20 (Sigma-Aldrich). Samples were then incubated overnight at 4°C under stirring with the primary antibodies, namely Mouse monoclonal anti-NESTIN [10C2] (Ab22035, Abcam; 1:200), Rabbit anti-βIII-Tubulin (ab18207, Abcam; 1:500), and Mouse monoclonal anti-MAP2 (Invitrogen, 13–1500; 1:200), diluted in PBS containing 1% NDS, 1% BSA, and 0.05% tween. After being rinsed trice with PBS containing 1% NDS, 1% BSA, and 0.05% tween, the samples were incubated with species-specific secondary antibodies (Alexa Fluor 647 donkey anti-mouse IgG. (H+L), Alexa Fluor 488 donkey anti-mouse IgG (H+L), and Alexa Fluor 647 donkey anti-rabbit IgG (H+L), all Invitrogen), diluted 1:500 in PBS containing 1% NDS, 1% BSA, and 0.05% tween for 60 min in the dark at room temperature. Finally, the samples were washed and counterstained with 0.15 μg/mL Hoechst 33342 in PBS for 20 min and mounted with Fluoromount Aqueous Mounting Medium (Sigma-Aldrich). Images were acquired using a Leica TCS SP5 Confocal Microscope, and subsequently analyzed using IMARIS software (version 10.2, Oxford Instruments).

4.30 | Immunocytometry Analysis of Developing and Mature Neurons

The expression of βIII-Tubulin and MAP2 after 12 days of differentiation under severely hypoxic environment in an absence and presence of catalase-coated oxygen-releasing hydrogel was assessed by immunocytometry [74]. Cells were isolated using nattokinase and Trypsin EDTA as described above and suspended in PBS. After counted, cells were stained with Zombie Aqua viability dye (BioLegend) for 15 min at room temperature. Subsequently, cells were washed and fixed in 1% w/v PFA in PBS for 20 min at 4°C, followed by incubation in blocking buffer (5% v/v normal goat serum; NGS, Biosource, in PBS) for 20 min. Cells were then incubated with primary antibodies, namely Rabbit anti-beta III tubulin (ab18207, Abcam) and Mouse anti-MAP2 (13-1500, Invitrogen) diluted 1:500 in PBS containing 1% v/v NGS for 30 min. After washing, cells were incubated with second antibodies, namely Alexa Fluor 488 donkey anti-mouse IgG (H+L) and Alexa Fluor 647 donkey anti-rabbit IgG (H+L), diluted 1:500 in PBS containing 1% v/v NGS for an additional 30 min. Cells were then washed trice, resuspended in FACS buffer (2% fetal bovine serum (FBS) and 0.1% w/v sodium azide), and analyzed by flow cytometry using a BD FACSCanto II, BD Biosciences (Becton Dickinson). Cellular debris was excluded on the basis of forward scatter (FSC) and side scatter (SSC) parameters. Viable cells were identified by exclusion of non-viable events using Zombie Aqua Fixable Viability Dye. Unstained samples and secondary antibody–only controls were included to define fluorescence gating strategies and to evaluate background signal and non-specific antibody binding, respectively (Figure S14). For each sample, at least 60 000 events were acquired. Quantification of marker-positive populations was performed within the gated live-cell population using software FlowJo v10.10 (BD Life Sciences, Ashland, OR, EUA).

4.31 | IMARIS Analysis

3D stack images of samples processed for Hoechst/ MAP2 labelling were used for analysis of neurosphere volume and neurite morphometry using Imaris (version 10.2, Oxford Instruments). The average volume of neurospheres was identified using Surfaces module (Figure S15). The Filament Tracer module was used to analyze neurite branching from individual neurospheres. The maximal neurite length was manually traced and measured using distance data from x-y plane in slice view, where at least 10 different neurites per image were analyzed. Filament full branch depth, and filament full branch level value were collected from the software (Figure S16). The averaged results were summarized from three independent experiments, with at least five different imaging positions analyzed for each experiment, and a minimum of 10 neurospheres were analyzed per image.

4.32 | Statistical Analysis

Statistical analysis was performed using GraphPad prism (version 10.1.2; GraphPad Software, Inc.) and ezANOVA software. Data are presented as mean ± standard deviation (SD). Comparisons between two related groups were performed using a two-tailed paired t-test. One-way or two-way analysis of variance (ANOVA) was used, followed by post hoc analysis with Tukey's, or Holm-Šídák multiple comparison tests. Comparison between two independent groups were performed using the non-parametric Mann-Whitney test using a 95% confidence interval was applied. A p value ≤ 0.05 was considered statistically significant.

Author Contributions

Sukulya Bunuasunthon: writing – original draft, visualization, validation, methodology, investigation, formal analysis, conceptualization. **Isabel F. Amaral**: writing – review & editing, validation, supervision, methodology, conceptualization. **Ana P. Pêgo**: writing – review, validation, supervision, resources, methodology, conceptualization. **Michiya Matsusaki**: writing – review & editing, validation, supervision, resources, project administration, methodology, funding acquisition, data curation, conceptualization. All authors edited the manuscript. All authors contributed to the design and implementation of the research and the analysis of results. All authors have seen and approved the final manuscript.

Acknowledgements

The authors would like to acknowledge Prof. T. Kida in The University of Osaka for providing access to the XRD instrumentation used in this study as well to two i3S scientific platforms: the Translational Cytometry Scientific Platform, in which flow cytometry analysis was conducted by Emília Cardoso, and the Bioimaging Scientific Platform, member of the PPBI (PPBI–POCI-01-0145-FEDER-022122). This study was financial supported by KAKENHI JP22H05131, JP22H05138, JP22H05140, JP22H05141, JP25H01220, JP22K21348, and JP21H04634 from Japan Society for Promotion of Science (JSPS). This study was also supported by COI-NEXT (JPMJPF2009) from Japan Science and Technology Agency (JST), JPNP231053211 and JPNP21502154-0 from New Engergy and Industrial Technology Development Organization (NEDO),

JPJSBP120239201, JPJSBP120252301, and Y2024L0906033 from JSPS, and the Air Force Office of Scientific Research, USA (Awards FA9550-20-1-0417 and FA9550-23-1-0599). APP acknowledges the MOBILIsE Project (no. 951723) from the European Union's Horizon 2020 research and innovation program and the MOBILIsE_Plus project, co-funded by the European Union through the NORTE 2030 Regional Program of the European Regional Development Fund (FEDER), under the operation with the code NORTE2030-FEDER-01801000.

Funding

JSPS KAKENHI (JP22H05131, JP22H05138, JP22H05140, JP22H05141, JP25H01220, JP22K21348, and JP21H04634) from JSPS, COI-NEXT (JPMJPF2009) from JST, JPNP231053211 and JPNP21502154-0 from NEDO, JPJSBP120239201, JPJSBP12025301, and Y2024L0906033 from JSPS and Air Force Office of Scientific Research, USA (Awards FA9550-20-1-0417 and FA9550-23-1-0599).

Conflicts of Interest

The authors declare no conflict of interest.

Data Availability Statement

The data that support the findings of this study are available from the corresponding author upon reasonable request.

References

1. B. Domínguez-Gil, N. L. Ascher, R. A. S. Fadhil, et al., "The Reality of Inadequate Patient Care and the Need for a Global Action Framework in Organ Donation and Transplantation," *Transplantation* 106 (2022): 2111–2117.

2. S. Li, X. Dan, H. Chen, et al., "Developing Fibrin-Based Biomaterials/Scaffolds in Tissue Engineering," *Bioactive Materials* 40 (2024): 597–623.

3. N. Sultana, A. Cole, and F. Strachan, "Biocomposite Scaffolds for Tissue Engineering: Materials, Fabrication Techniques and Future Directions," *Materials* 17 (2024): 5577.

4. M. Kasturi, V. Mathur, M. Gadre, V. Srinivasan, and K. S. Vasanthan, "Three Dimensional Bioprinting for Hepatic Tissue Engineering: From In Vitro Models to Clinical Applications," *Tissue Engineering and Regenerative Medicine* 21 (2024): 21–52.

5. M. Hirao, J. Hashimoto, N. Yamasaki, et al., "Oxygen Tension is an Important Mediator of the Transformation of Osteoblasts to Osteocytes," *Journal of Bone and Mineral Metabolism* 25 (2007): 266–276.

6. P. Abdollahiyan, F. Oroojalian, and A. Mokhtarzadeh, "The Triad of Nanotechnology, Cell Signalling, and Scaffold Implantation for the Successful Repair of Damaged Organs: An Overview on Soft-Tissue Engineering," *Journal of Controlled Release* 332 (2021): 460–492.

7. C. Bergemann, P. Elter, R. Lange, et al., "Cellular Nutrition in Complex Three-Dimensional Scaffolds: A Comparison Between Experiments and Computer Simulations," *International Journal of Biomaterials* 2015 (2015): 1–12.

8. C. Reily, T. J. Stewart, M. B. Renfrow, and J. Novak, "Glycosylation in Health and Disease," *Nature Reviews Nephrology* 15 (2019): 346–366.

9. F. Dehghani and N. Annabi, "Engineering Porous Scaffolds Using Gas-Based Techniques," *Current Opinion in Biotechnology* 22 (2011): 661–666.

10. M. Lovett, K. Lee, A. Edwards, and D. L. Kaplan, "Vascularization Strategies for Tissue Engineering," *Tissue Engineering Part B: Reviews* 15 (2009): 353–370.

11. H. Sekine and T. Okano, "Capillary Networks for Bio-Artificial Three-Dimensional Tissues Fabricated Using Cell Sheet Based Tissue Engineering," *International Journal of Molecular Sciences* 22 (2020): 92.

12. A. L. Farris, A. N. Rindone, and W. L. Grayson, "Oxygen Delivering Biomaterials for Tissue Engineering," *Journal of Materials Chemistry B* 4 (2016): 3422–3432.

13. Y. Hu, X. Wang, P. Zhao, H. Wang, W. Gu, and L. Ye, "Nanozyme-Catalyzed Oxygen Release From Calcium Peroxide Nanoparticles for Accelerated Hypoxia Relief and Image-Guided Super-Efficient Photodynamic Therapy," *Biomaterials Science* 8 (2020): 2931–2938.

14. X. Sun, F. Yao, H. Zhang, and J. Li, "Oxygen-Generating Materials and Their Biomedical Applications: A Review," *Journal of Materials Science* 57 (2022): 9077–9103.

15. A. Rastinfard, B. Dalisson, and J. Barralet, "Aqueous Decomposition Behavior of Solid Peroxides: Effect of pH and Buffer Composition on Oxygen and Hydrogen Peroxide Formation," *Acta Biomaterialia* 145 (2022): 390–402.

16. M. Y. Mollajavadi, M. Saadatmand, and F. Ghobadi, "Effect of Calcium Peroxide Particles as Oxygen-Releasing Materials on Cell Growth and Mechanical Properties of Scaffolds for Tissue Engineering," *Iranian Polymer Journal* 32 (2023): 599–608.

17. N. Li, X. Lu, Y. Yang, et al., "Calcium Peroxide-Based Hydrogel Patch With Sustainable Oxygenation for Diabetic Wound Healing," *Advanced Healthcare Materials* 13 (2024): 2303314.

18. G. Camci-Unal, N. Alemdar, N. Annabi, and A. Khademhosseini, "Oxygen-Releasing Biomaterials for Tissue Engineering," *Polymer International* 62 (2013): 843–848.

19. N. G. A. Willemen, S. Hassan, M. Gurian, et al., "Oxygen-Releasing Biomaterials: Current Challenges and Future Applications," *Trends in Biotechnology* 39 (2021): 1144–1159.

20. R. Augustine, M. Gezek, N. S. Bostanci, A. Nguyen, and G. Camci-Unal, "Oxygen-Generating Scaffolds: One Step Closer to the Clinical Translation of Tissue Engineered Products," *Chemical Engineering Journal* 455 (2023): 140783.

21. H.-Y. Liang, W.-K. Lee, J.-T. Hsu, et al., "Polycaprolactone in Bone Tissue Engineering: A Comprehensive Review of Innovations in Scaffold Fabrication and Surface Modifications," *Journal of Functional Biomaterials* 15 (2024): 243.

22. L. E. Smith, S. Rimmer, and S. MacNeil, "Examination of the Effects of Poly(N-Vinylpyrrolidinone) Hydrogels in Direct and Indirect Contact With Cells," *Biomaterials* 27 (2006): 2806–2812.

23. J. I. Kang, K. M. Park, and K. D. Park, "Oxygen-Generating Alginate Hydrogels as a Bioactive Acellular Matrix for Facilitating Wound Healing," *Journal of Industrial and Engineering Chemistry* 69 (2019): 397–404.

24. C. Lennicke, J. Rahn, R. Lichtenfels, L. A. Wessjohann, and B. Seliger, "Hydrogen Peroxide—Production, Fate and Role in Redox Signaling of Tumor Cells," *Cell Communication and Signaling* 13 (2015): 39.

25. M. Alfonso-Prieto, P. Vidossich, and C. Rovira, "The Reaction Mechanisms of Heme Catalases: An Atomistic View by Ab Initio Molecular Dynamics," *Archives of Biochemistry and Biophysics* 525 (2012): 121–130.

26. S. I. H. Abdi, J. Y. Choi, H. C. Lau, and J. O. Lim, "Controlled Release of Oxygen From PLGA-Alginate Layered Matrix and its In Vitro Characterization on the Viability of Muscle Cells Under Hypoxic Environment," *Tissue Engineering and Regenerative Medicine* 10 (2013): 131–138.

27. S. I. H. Abdi, S. M. Ng, and J. O. Lim, "An Enzyme-Modulated Oxygen-Producing Micro-System for Regenerative Therapeutics," *International Journal of Pharmaceutics* 409 (2011): 203–205.

28. S. Park and K. M. Park, "Hyperbaric Oxygen-Generating Hydrogels," *Biomaterials* 182 (2018): 234–244.

29. M. J. Han, J. A. An, J. M. Kim, D. N. Heo, I. K. Kwon, and K. M. Park, "Calcium Peroxide-Mediated Bioactive Hydrogels for Enhanced Angiogenic Paracrine Effect and Osteoblast Proliferation," *Journal of Industrial and Engineering Chemistry* 120 (2023): 121–130.

30. B. Newland, M. Baeger, D. Eigel, H. Newland, and C. Werner, "Oxygen-Producing Gellan Gum Hydrogels for Dual Delivery of Either Oxygen or Peroxide With Doxorubicin," *ACS Biomaterials Science & Engineering* 3 (2017): 787–792.

31. D. Tomioka, S. Fujita, J. Groll, and M. Matsusaki, "Hydroxyapatite Nanocoating on Calcium Peroxide Microparticles for Sustained Oxygen Release," *Chemistry of Materials* 35 (2023): 5378–5391.

32. S. Bunuasunthon, M. Nakamoto, V. P. Hoven, and M. Matsusaki, "Construction of Tough Hydrogel Cross-Linked via Ionic Interaction by Protection Effect of Hydrophobic Domains," *ACS Biomaterials Science & Engineering* 10 (2024): 4245–4258.

33. E. Boanini, M. Gazzano, K. Rubini, and A. Bigi, "Composite Nanocrystals Provide New Insight on Alendronate Interaction With Hydroxyapatite Structure," *Advanced Materials* 19 (2007): 2499–2502.

34. M. Schrader and H. D. Fahimi, "Peroxisomes and Oxidative Stress," *Biochimica et Biophysica Acta (BBA)—Molecular Cell Research* 1763 (2006): 1755–1766.

35. J. I. Kang and K. M. Park, "Oxygen-Supplying Syringe to Create Hyperoxia-Inducible Hydrogels for In Situ Tissue Regeneration," *Biomaterials* 293 (2023): 121943.

36. Z. Ivanovic, "Hypoxia or In Situ Normoxia: The Stem Cell Paradigm," *Journal of Cellular Physiology* 219 (2009): 271–275.

37. L. C. O'Brien, P. M. Keeney, and J. P. Bennett, "Differentiation of Human Neural Stem Cells into Motor Neurons Stimulates Mitochondrial Biogenesis and Decreases Glycolytic Flux," *Stem Cells and Development* 24 (2015): 1984.

38. J. Van Den Ameele and A. H. Brand, "Neural Stem Cell Temporal Patterning and Brain Tumour Growth Rely on Oxidative Phosphorylation," *eLife* 8 (2019): 47887.

39. A. M. Sheikh, S. Hossain, and S. Tabassum, "Advances in Stem Cell Therapy for Stroke: Mechanisms, Challenges, and Future Directions," *Regenerative Medicine Reports* 1 (2024): 76–92.

40. D. A. Ossipov, "Bisphosphonate-Modified Biomaterials for Drug Delivery and Bone Tissue Engineering," *Expert Opinion on Drug Delivery* 12 (2015): 1443–1458.

41. C.-C. Wong, C.-X. Lu, E.-C. Cho, et al., "Calcium Peroxide Aids Tyramine-Alginate Gel to Crosslink With Tyrosinase for Efficient Cartilage Repair," *International Journal of Biological Macromolecules* 208 (2022): 299–313.

42. C. Gao, Y. Huang, L. Zhang, et al., "Self-Reinforcement Hydrogel With Sustainable Oxygen-Supply for Enhanced Cell Ingrowth and Potential Tissue Regeneration," *Biomaterials Advances* 141 (2022): 213105.

43. F. Topuz, A. Henke, W. Richtering, and J. Groll, "Magnesium Ions and Alginate do Form Hydrogels: A Rheological Study," *Soft Matter* 8 (2012): 4877.

44. T. Qu, G. Nan, Y. Ouyang, et al., "Structure–Property Relationship, Glass Transition, and Crystallization Behaviors of Conjugated Polymers," *Polymers* 15 (2023): 4268.

45. R. Noriega, J. Rivnay, K. Vandewal, et al., "A General Relationship Between Disorder, Aggregation and Charge Transport in Conjugated Polymers," *Nature Materials* 12 (2013): 1038–1044.

46. W. H. Park, "The Effects of Exogenous H_2O_2 on Cell Death, Reactive Oxygen Species and Glutathione Levels in Calf Pulmonary Artery and Human Umbilical Vein Endothelial Cells," *International Journal of Molecular Medicine* 31 (2013): 471–476.

47. T. Chidawanyika and S. Supattapone, "Hydrogen Peroxide-Induced Cell Death in Mammalian Cells," *Journal of Cell Communication and Signaling* 2 (2021): 206–211, 10.33696/Signaling.2.052.

48. S. H. Oh, C. L. Ward, A. Atala, J. J. Yoo, and B. S. Harrison, "Oxygen Generating Scaffolds for Enhancing Engineered Tissue Survival," *Biomaterials* 30 (2009): 757–762.

49. N. Alemdar, J. Leijten, G. Camci-Unal, et al., "Oxygen-Generating Photo-Cross-Linkable Hydrogels Support Cardiac Progenitor Cell Survival by Reducing Hypoxia-Induced Necrosis," *ACS Biomaterials Science & Engineering* 3 (2017): 1964–1971.

50. E. Pedraza, M. M. Coronel, C. A. Fraker, C. Ricordi, and C. L. Stabler, "Preventing Hypoxia-Induced Cell Death in Beta Cells and Islets via Hydrolytically Activated, Oxygen-Generating Biomaterials," *Proceedings of the National Academy of Sciences* 109 (2012): 4245–4250.

51. M. Zielińska-Przyjemska, A. Olejnik, A. Dobrowolska-Zachwieja, M. Łuczak, and W. Baer-Dubowska, "DNA Damage and Apoptosis in Blood Neutrophils of Inflammatory Bowel Disease Patients and in Caco-2 Cells In Vitro Exposed To Betanin," *Postępy Higieny i Medycyny Doświadczalnej* 70 (2016): 265–271.

52. D. Kovács, V. B. Vántus, E. Vámos, et al., "Olaparib: A Clinically Applied PARP Inhibitor Protects From Experimental Crohn's Disease and Maintains Barrier Integrity by Improving Bioenergetics Through Rescuing Glycolysis in Colonic Epithelial Cells," *Oxidative Medicine and Cellular Longevity* 2021 (2021): 7308897.

53. S. Akagi, K. Nakamura, M. Kondo, et al., "Evidence for Hypoxia-Induced Shift in ATP Production From Glycolysis to Mitochondrial Respiration in Pulmonary Artery Smooth Muscle Cells in Pulmonary Arterial Hypertension," *Journal of Clinical Medicine* 12 (2023): 5028.

54. E. Zoneff, Y. Wang, C. Jackson, et al., "Controlled Oxygen Delivery to Power Tissue Regeneration," *Nature Communications* 15 (2024): 4361.

55. S. Zhang, M. Hosaka, T. Yoshihara, et al., "Phosphorescent Light–Emitting Iridium Complexes Serve as a Hypoxia-Sensing Probe for Tumor Imaging in Living Animals," *Cancer Research* 70 (2010): 4490–4498.

56. E. Jablonská, J. Kubásek, D. Vojtěch, T. Ruml, and J. Lipov, "Test Conditions can Significantly Affect the Results of In Vitro Cytotoxicity Testing of Degradable Metallic Biomaterials," *Scientific Reports* 11 (2021): 6628.

57. G. H. Malthankar-Phatak, A. B. Patel, Y. Xia, et al., "Effects of Continuous Hypoxia on Energy Metabolism in Cultured Cerebro-Cortical Neurons," *Brain Research* 1229 (2008): 147–154.

58. L. De Filippis and D. Delia, "Hypoxia in the Regulation of Neural Stem Cells," *Cellular and Molecular Life Sciences* 68 (2011): 2831–2844.

59. R. D. Guzy and P. T. Schumacker, "Oxygen Sensing by Mitochondria at Complex III: The Paradox of Increased Reactive Oxygen Species During Hypoxia," *Experimental Physiology* 91 (2006): 807–819.

60. B. H. Jiang, G. L. Semenza, C. Bauer, and H. H. Marti, "Hypoxia-Inducible Factor 1 Levels Vary Exponentially Over a Physiologically Relevant Range of O_2 Tension," *American Journal of Physiology-Cell Physiology* 271 (1996): C1172.

61. Y. Fan, J. Li, and B. Fang, "A Tale of Two: When Neural Stem Cells Encounter Hypoxia," *Cellular and Molecular Neurobiology* 43 (2023): 1799–1816.

62. S. R. L. Stacpoole, B. Bilican, D. J. Webber, et al., "Derivation of Neural Precursor Cells From Human ES Cells at 3% O_2 is Efficient, Enhances Survival and Presents No Barrier to Regional Specification And Functional Differentiation," *Cell Death & Differentiation* 18 (2011): 1016–1023.

63. A. Kaminska, K. Radoszkiewicz, P. Rybkowska, A. Wedzinska, and A. Sarnowska, "Interaction of Neural Stem Cells (NSCs) and Mesenchymal Stem Cells (MSCs) as a Promising Approach in Brain Study and Nerve Regeneration," *Cells* 11 (2022): 1464.

64. M. M. Daadi, A.-L. Maag, and G. K. Steinberg, "Adherent Self-Renewable Human Embryonic Stem Cell-Derived Neural Stem Cell Line: Functional Engraftment in Experimental Stroke Model," *PLoS ONE* 3 (2008): 1644.

65. C. Buhnemann, A. Scholz, C. Bernreuther, et al., "Neuronal Differentiation of Transplanted Embryonic Stem Cell-Derived Precursors in Stroke Lesions of Adult Rats," *Brain* 129 (2006): 3238–3248.

66. Y. Yun, D. Baek, D. Lee, et al., "Combined Method of Neuronal Cell-Inducible Vector and Valproic Acid for Enhanced Gene Expression Under Hypoxic Conditions," *Tissue Engineering and Regenerative Medicine* 17 (2020): 55–66.

67. G. Tarricone, I. Carmagnola, and V. Chiono, "Tissue-Engineered Models of the Human Brain: State-of-the-Art Analysis and Challenges," *Journal of Functional Biomaterials* 13 (2022): 146.

68. R. Duquette, S. P. Salazar, Z. Z. Wang, A. Sohrabi, and S. K. Seidlits, "Systematic Investigation of the Effects of Neural Stem Cell Spheroid Size and Density on Fate Specification in 3D Culture," *Journal of Materials Chemistry B* 14 (2026): 2014–2027.

69. J. Khodaveisi, H. Banejad, A. Afkhami, E. Olyaie, S. Lashgari, and R. Dashti, "Synthesis of Calcium Peroxide Nanoparticles as an Innovative Reagent for In Situ Chemical Oxidation," *Journal of Hazardous Materials* 192 (2011): 1437–1440.

70. D. Tomioka, S. A. Jung, A. Pich, and M. Matsusaki, "Fabrication of Oxygen-Releasing Dextran Microgels by Droplet-Based Microfluidic Method," *Royal Society of Chemistry Advances* 14 (2024): 26544.

71. S. Lee, D.-W. Lee, N. Rajput, T. Levato, A. Shanti, and T.-Y. Kim, "3D-Printed Microcubes for Catalase Drug Delivery," *American Chemical Society Omega* 8 (2023): 26775.

72. M. Piantino, D.-H. Kang, T. Furihata, et al., "Development of a Three-Dimensional Blood-Brain Barrier Network With Opening Capillary Structures for Drug Transport Screening Assays," *Materials Tomonth Bio* 15 (2022): 100324.

73. D. Barros, E. Conde-Sousa, A. M. Gonçalves, et al., "Engineering Hydrogels With Affinity-Bound Laminin as 3D Neural Stem Cell Culture Systems," *Biomaterials Science* 7 (2019): 5338–5349.

74. J. Loureiro, A. L. Torres, T. Neto, et al., "Conjugation of the T1 Sequence From CCN1 to Fibrin Hydrogels for Therapeutic Vascularization," *Materials Science and Engineering: C* 104 (2019): 109847.

Supporting Information

Additional supporting information can be found online in the Supporting Information section.

Supporting File 1: adma73635-sup-0001-SuppMat.pdf.

Supporting File 2: adma73635-sup-0002-MovieS1.mov.

Supporting File 3: adma73635-sup-0003-MovieS2.mp4.

Supporting File 4: adma73635-sup-0004-MovieS3.mp4.

Supporting File 5: adma73635-sup-0005-MovieS4.mp4.